RESEARCH MEMORANDUM

STATIC LONGITUDINAL AND LATERAL STABILITY PARAMETERS OF THREE FLARED-SKIRT TWO-STAGE MISSILE CONFIGURATIONS AT A MACH NUMBER OF 6.86

By Jim A. Penland and C. Maria Carroll

Langley Aeronautical Laboratory
Langley Field, Va.

NATIONAL ADVISORY COMMITTEE
FOR AERONAUTICS

WASHINGTON
June 5, 1957

NATIONAL ADVISORY COMMITTEE FOR AERONAUTICS

RESEARCH MEMORANDUM

STATIC LONGITUDINAL AND LATERAL STABILITY PARAMETERS OF THREE FLARED-SKIRT TWO-STAGE MISSILE CONFIGURATIONS AT A MACH NUMBER OF 6.86

By Jim A. Penland and C. Maria Carroll

SUMMARY

An investigation to determine the static longitudinal and lateral stability of three variations of a flared-skirt-type two-stage missile configuration with different nose shapes, body cross sections, and skirt geometry has been carried out in the Langley 11-inch hypersonic tunnel.

The tests were made at a Mach number of 6.86 and a range of Reynolds numbers from 1.69×10^6 to 5.1×10^6 based on body length. Six-component force data were obtained for angles of attack from -5° to 15° and angles of roll of 0° to 60°.

The results of the investigation show that the models having rounded triangular cross sections have a variation of lift, drag, lift-drag ratio, and stability with roll angle. The variable Reynolds number tests show that with an increase in Reynolds number the drag decreases and the stability and lift-drag ratio increases. A hemispherical nose increases the drag, decreases the lift-drag ratio, and increases the longitudinal stability as compared to a 60° blunt conical nose.

INTRODUCTION

The possible high rate of heat transfer on the leading edges of conventional vertical- and horizontal-tail surfaces at hypersonic speeds makes it necessary to explore the use of other stability-producing devices. One such device is the flared skirt (refs. 1 and 2) on which the heating problem is less severe and yet it is capable of providing both longitudinal as well as lateral stability at high Mach numbers without markedly increasing the weight of the missile.

An investigation has been conducted to determine the static stability characteristics of three two-stage missile configurations, each stage incorporating a flared-skirt type of afterbody. Two of the configurations are of the minimum-weight type which uses only a thin retaining skin over three rocket boosters so that the first-stage body is given a round-cornered triangular cross section. The body and the flared afterbody of the third configuration had circular cross-sectional shapes.

This paper presents the static longitudinal and lateral characteristics for these configurations through an angle-of-attack range of -5° to 15° at a Mach number of 6.86. Some effects of roll angle, variation of Reynolds number, and change in nose shape on the aerodynamic characteristics are also presented.

COEFFICIENTS AND SYMBOLS

C_L lift coefficient, $\frac{F_L + F_{bp} \sin \alpha}{qS}$

C_D drag coefficient, $\frac{F_D' + F_{bp} \cos \alpha}{qS}$

C_Y side-force coefficient, F_Y/qS

C_N normal-force coefficient, F_N/qS

C_m pitching-moment coefficient, M_Y/qSb

C_n yawing-moment coefficient, M_Z/qSb

C_l rolling-moment coefficient, M_X/qSb

x_{cp} center of pressure, $\frac{x_{cg}}{b} - \frac{C_m}{C_N}$, percent body length from nose

$F_L = F_N \cos \alpha - F_A \sin \alpha$

$F_D' = F_N \sin \alpha + F_A \cos \alpha$

F_Y force along Y-axis

F_N force along Z-axis

F_A	force along X-axis
M_X	moment about X-axis
M_Y	moment about Y-axis
M_Z	moment about Z-axis
F_{bp}	base-pressure correction, $(p_\infty - p_{bp})S_b$
q	free-stream dynamic pressure
R	Reynolds number
S	cross-sectional area of body of first stage
S_b	area of base of first stage
b	length of body
x_{cg}	location of center of gravity
M	Mach number
p_∞	free-stream static pressure
p_{bp}	pressure on base of first stage
α	angle of attack, deg

MODELS

The models used for the present tests may be seen in the photographs (figs. 1 and 2) and the detail drawing (fig. 3). The 60° blunt conical nose was interchanged with the hemispherical nose for tests to determine the variation of forces and moments with nose bluntness.

The overall length of each of the three configurations is the same for any one nose shape, but the substitution of the hemispherical nose shortens each model by 0.25 inch. The basic angle of skirt flare for model 1-A is 10° and for models 1-B and 1-C, 12°. This variation in the flare of the skirt makes the base area of model 1-A 27 percent smaller than that of models 1-B and 1-C. The cross-sectional area of the first stage of each configuration is constant although the cross-sectional shape of the first stage of configurations 1-A and 1-B is triangular,

[redacted]

[redacted]

whereas the first stage of configuration 1-C is circular. This constant cross-sectional body area of the first stage was used as the reference area for the calculation of the force and moment coefficients. The skirts of model 1-A consist of a transition from a circular cross section on the second stage to a round-cornered triangular cross section on the first stage, and a transition from the round-cornered triangle of the first stage to the circular base. The second-stage skirt of model 1-B is identical to the corresponding skirt of 1-A, but the first-stage or rear skirt of 1-B consists of a frustrum of a cone that is faired to the semitriangular first-stage body. The skirts of configuration 1-C are both frustrums of cones.

The models were machined from steel. An indexing insert, that fitted between the model and the balance, was used to locate the model at angles of roll with respect to the axes of the balance (fig. 4).

APPARATUS AND TESTS

The tests were conducted in the Langley 11-inch hypersonic blowdown tunnel with the models installed in the test section as shown in figure 1. The tests were made at an average Mach number of 6.86 at stagnation pressures of 11, 21, and 31 atmospheres absolute and the average stagnation temperature was regulated to 675° F to avoid liquefaction (ref. 3). The Reynolds number based upon body length corresponding to these stagnation pressures was 0.11×10^6, 0.21×10^6, and 0.31×10^6 per inch, respectively. The absolute humidity was kept to less than 1.9×10^{-5} pounds of water per pound of dry air for all tests. Force and moment data were obtained by use of a six-component strain-gage force balance through an angle-of-attack range of approximately -5° to 15° at roll angles from 0° to 60°. The balance and model were mounted in the tunnel test section on a movable strut which was rotated through an angle of attack during the run for each test point. During each run the period of constant Mach number flow was sufficiently long (approximately 1 minute) to permit testing the models at several angles of attack. The angles of attack were measured optically from schlieren photographs. Model base pressures were measured during all tests and the axial-force component was adjusted to correspond to a base pressure equal to stream static pressure.

ACCURACY OF DATA

The maximum uncertainties in the force and moment coefficients for the individual test points due to the force balance system are presented as follows.

Coefficient	Stagnation pressures, atmospheres		
	11±0.033	21±0.053	31±0.08
C_N, C_L	±0.113	±0.059	±0.040
C_D	±.018	±.009	±.006
C_Y	±.035	±.018	±.013
C_m	±.014	±.007	±.005
C_l	±.003	±.002	±.001
C_n	±.006	±.003	±.002

The reading accuracy of the angle of attack was ±0.10° and the variation of Mach number was no greater than ±0.01.

PRESENTATION OF RESULTS

The longitudinal characteristics are referred to the stability-axis system, and the lateral characteristics are referred to the body-axis system. (See fig. 5.) The results are presented in the following order:

[redacted]

RESULTS AND DISCUSSION

Model 1-A.- A comparison of the longitudinal characteristics of model 1-A for various angles of roll is presented in figure 9. It should be noted that a flat portion of the semitriangular body faced downward at a roll angle of 0° and that a round corner faced downward at an angle of roll of 60° (fig. 4). The difference in the aerodynamic loading seen in figure 9(a) on the model at different roll angles follows from the change in the shape of that portion of the body that faces the flow at angle of attack as the model is rotated about its body axis. This variation in loading, that is, the decrease in lift and drag on the rear portion of the configuration causes a slight forward shift of the center of pressure with an accompanying decrease in longitudinal stability at angles of attack above 5°. Figure 9(b) shows that this loss in lift, with increasing roll angle, results in a decrease in lift-drag ratio. A discussion of the effectiveness of a flat-bottomed body in producing lift at hypersonic speeds may be found in reference 4.

A comparison of the longitudinal characteristics of model 1-A for Reynolds numbers of 1.7×10^6, 3.4×10^6, and 5.1×10^6 based on body length and at a roll angle of 0° is presented in figure 10. It should be noted that the overall drag decreases as the Reynolds number increases and, conversely, the longitudinal stability increases as the Reynolds number increases. These effects are probably due to the thinning of the boundary layer as the Reynolds number increases and to the associated increase in efficiency of the flared skirts as producers of negative pitching moments. The maximum value of lift-drag ratio (fig. 10(b)) increases noticeably with the increase in Reynolds number.

A comparison of the longitudinal characteristics of model 1-A with a blunt 60° conical nose and model 1-Ah which has a hemispherical nose is presented in figure 11. It may be seen that both the drag and the stability are increased by the use of the hemispherical nose. The increase in stability of model 1-Ah compared with that of model 1-A is partly due to the decrease in the nose length forward of the moment reference. The lift-drag ratio (fig. 11(b)) was markedly decreased with the addition of the hemispherical nose. A schlieren photograph of model 1-Ah may be seen in figure 12(f).

An additional test was made on model 1-A in an effort to fix transition by use of a series of small wires protruding radially from the round second-stage body. The only variation in the results was an increase in the drag of the configuration and no change in flare effectiveness was apparent as would be expected if the transition had been tripped by the protuberances.

A comparison of the lateral stability characteristics of model 1-A for various angles of roll is presented in figure 13. The changes in rolling moment with roll angle are very small for the angle-of-attack range tested because the resultant forces on each of the flat surfaces passes through the body center line. The positive increase of side force and the negative increase of yawing moment with angle of attack for angles of roll between 0° and 30° follows from the angular movement of the flat bottom surfaces as the model is rolled. The side force and yaw should be zero for roll angles of 0° and 60° because of symmetry in x, z plane in these positions. (See fig. 4.) Because of this variation of forces and moments with roll angle, operation along a predetermined path of a missile with this type of cross section could be difficult with only aerodynamic stabilization at this Mach number and Reynolds number.

Model 1-B.- Model 1-B was not tested with as many variables as was model 1-A; the comparisons of the longitudinal and lateral characteristics of model 1-B with angles of roll of 0°, 30°, and 60° are presented in figures 14 and 15, respectively. It may be seen by comparing figures 9 and 14 that model 1-B is considerably more stable longitudinally than model 1-A because of the larger angle of skirt flare. The semitriangular body gives the same trend of decreasing lift and drag with roll angle but the configuration exhibits increased stability for the higher roll angles which is opposite to the trend shown by model 1-A. The side force (fig. 15) is considerably less at a roll angle of 30° than the side force for the corresponding angle for model 1-A, primarily because of the elimination of the flattened area on the flared skirt and somewhat by a thickening of the boundary layer ahead of the skirt-attachment point because of the increase of the skirt-flare angle from 7° on model 1-A to 12° on model 1-B.

Model 1-C.- A comparison of the longitudinal characteristics of configuration 1-C with a 60° blunt conical nose and a hemispherical nose is presented in figure 17. The tests with the hemispherical nose indicate an increase in drag and longitudinal stability over the 60° blunt-nose model with the lift remaining approximately the same. As with model 1-Ah, this increase in stability with the hemispherical nose is partly due to the decrease in the length of the model ahead of the moment center. The increase in drag decreases the lift-drag ratio as may be seen in figure 17(b).

CONCLUDING REMARKS

A comparison of the results of the various model tests in the Langley 11-inch hypersonic tunnel at a Mach number 6.86 showed that models having a semitriangular cross section exhibit a variation of lift, drag, lift-drag ratio, and stability with roll angle. The variable Reynolds number tests show, as would be expected for laminar flow, that the overall drag decreases and that the longitudinal stability and lift-drag ratio increase with an increase of Reynolds number. A comparison of the tests of the models equipped with a 60° blunt conical nose and those of the models equipped with a hemispherical nose show that the hemispherical nose increases the drag, decreases the lift-drag ratio, and increases the longitudinal stability.

Langley Aeronautical Laboratory,
National Advisory Committee for Aeronautics,
Langley Field, Va., March 25, 1957.

REFERENCES

1. Alley, D. J.: A Supersonic Body Profile Development Study. Rep. No. 6 - The Results of a Theoretical Study of Six Flared-Tailed Bodies of Revolution and Their Modifications. UMM-76 (USAF Contract W-33-038-ac-1422.), Univ. of Michigan, Willow Run Res. Center, Jan. 1951.

2. Eggers, A. J., Jr., and Syvertson, Clarence A.: Experimental Investigation of a Body Flare for Obtaining Pitch Stability and a Body Flap for Obtaining Pitch Control in Hypersonic Flight. NACA RM A54J13, 1955.

3. McLellan, Charles H., and Williams, Thomas W.: Liquefaction of Air in the Langley 11-Inch Hypersonic Tunnel. NACA TN 3302, 1954.

4. Ridyard, Herbert W.: The Aerodynamic Characteristics of Two Series of Lifting Bodies at Mach Number 6.86. NACA RM L54C15, 1954.

[redacted]

[redacted]

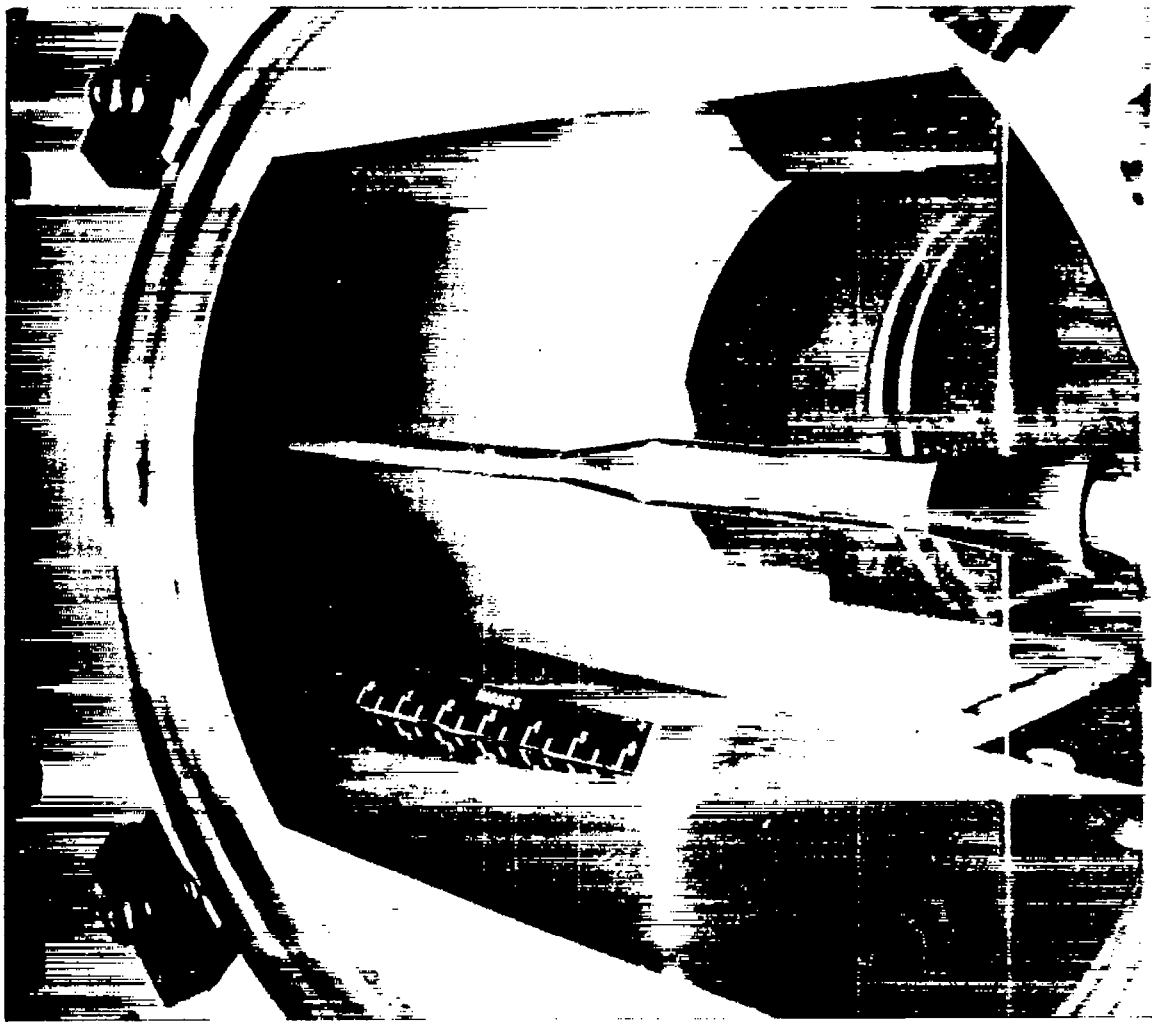

L-91793

Figure 1.- Photograph of model 1-A installed in the Langley 11-inch hypersonic tunnel test section. Roll angle, 0°.

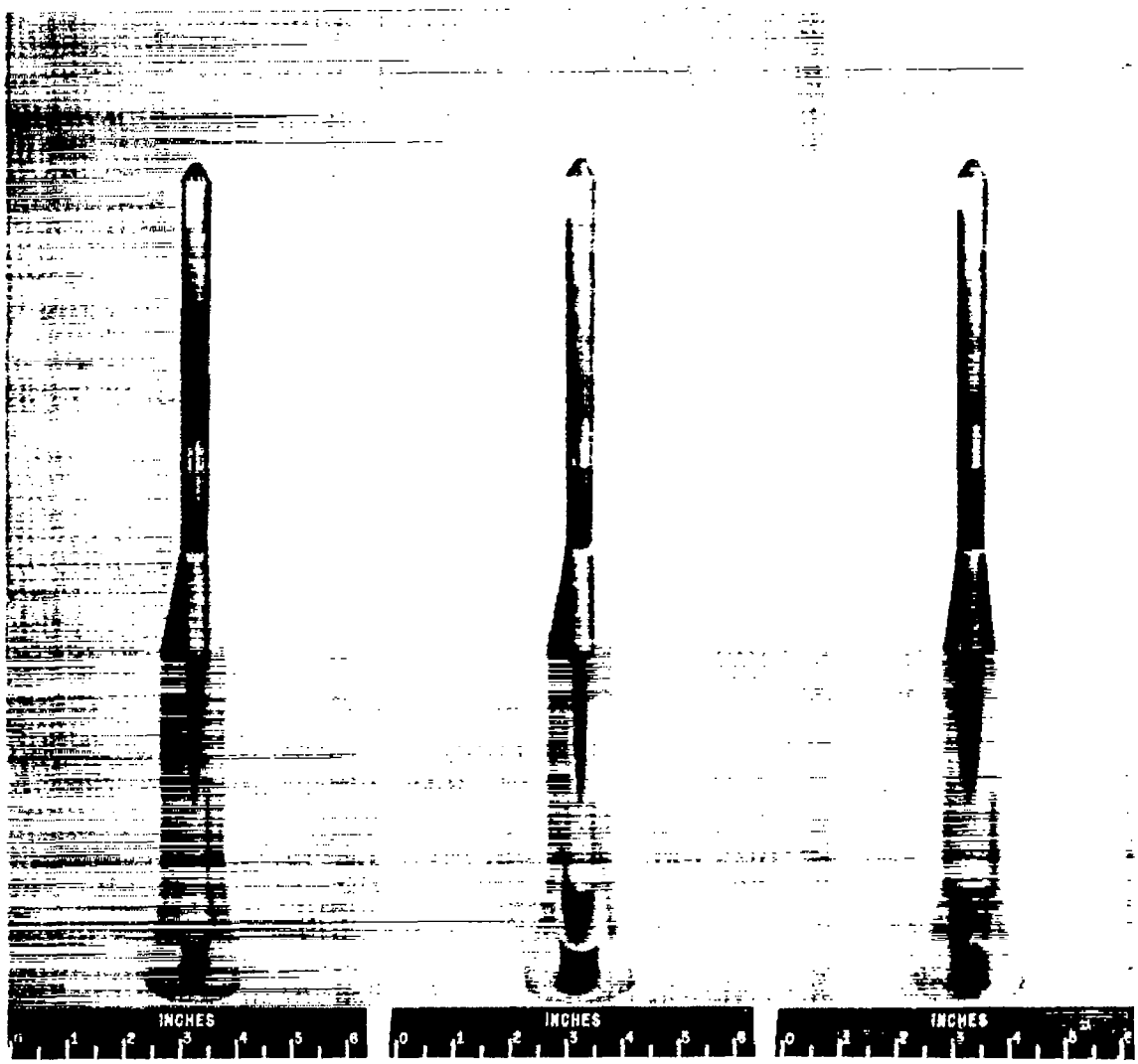

L-57-188

(a) Model 1-A. (b) Model 1-B. (c) Model 1-C.

Figure 2.- Photographs of the three configurations tested.

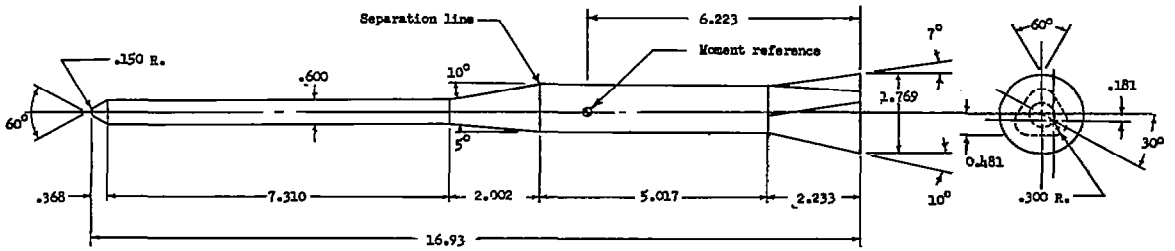

(a) Model 1-A.

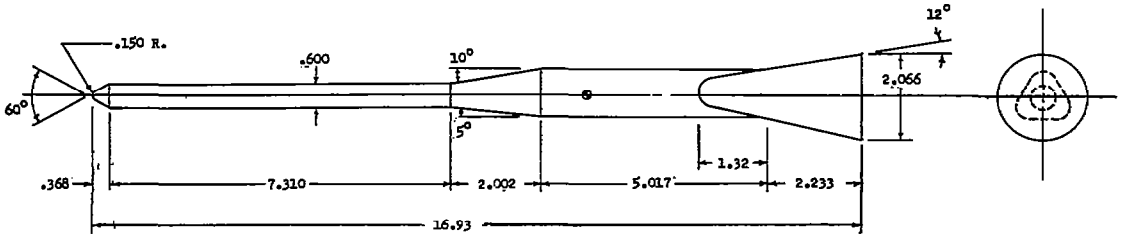

(b) Model 1-B.

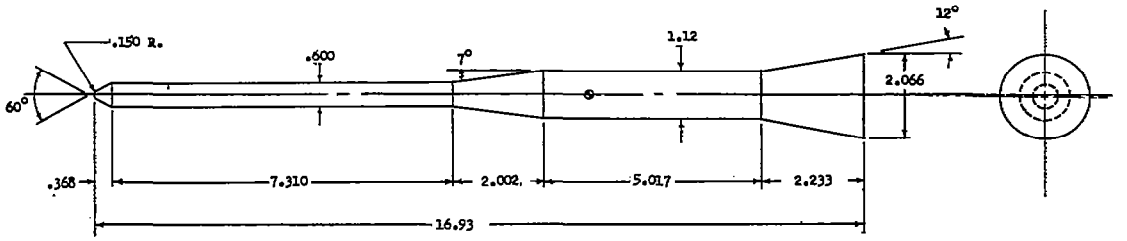

(c) Model 1-C.

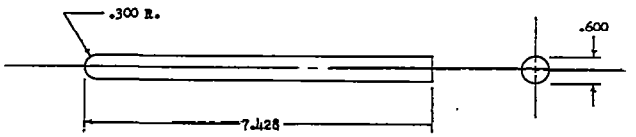

(d) Detachable hemispherical nose, denoted by postscript h.

Figure 3.- Details and basic dimensions of flared-skirt models. All dimensions are in inches.

(a) Roll angle 0°.

(b) Roll angle 15°.

(c) Roll angle 30°.

(d) Roll angle 60°.

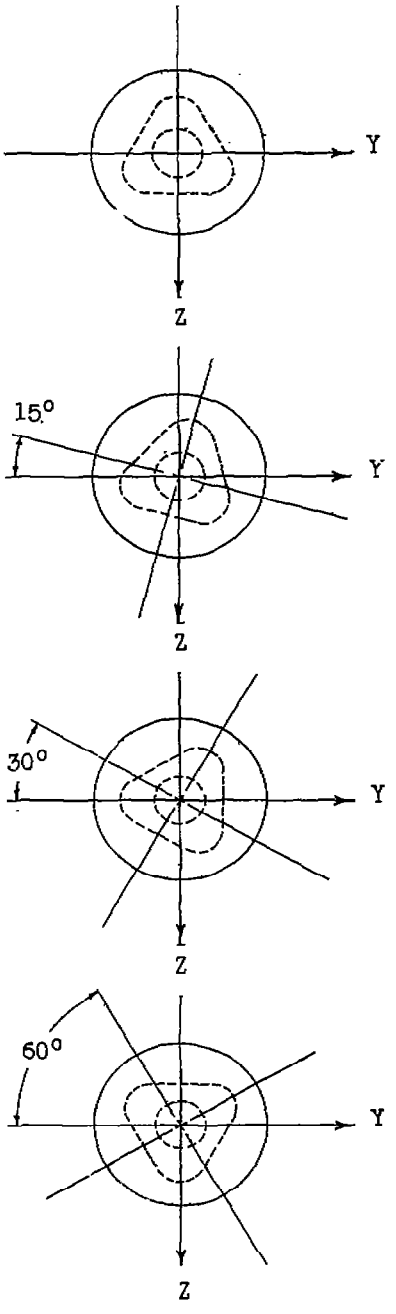

Figure 4.- Schematic views from downstream of models 1-A and 1-B showing relation of semitriangular body to the axis system for various roll angles.

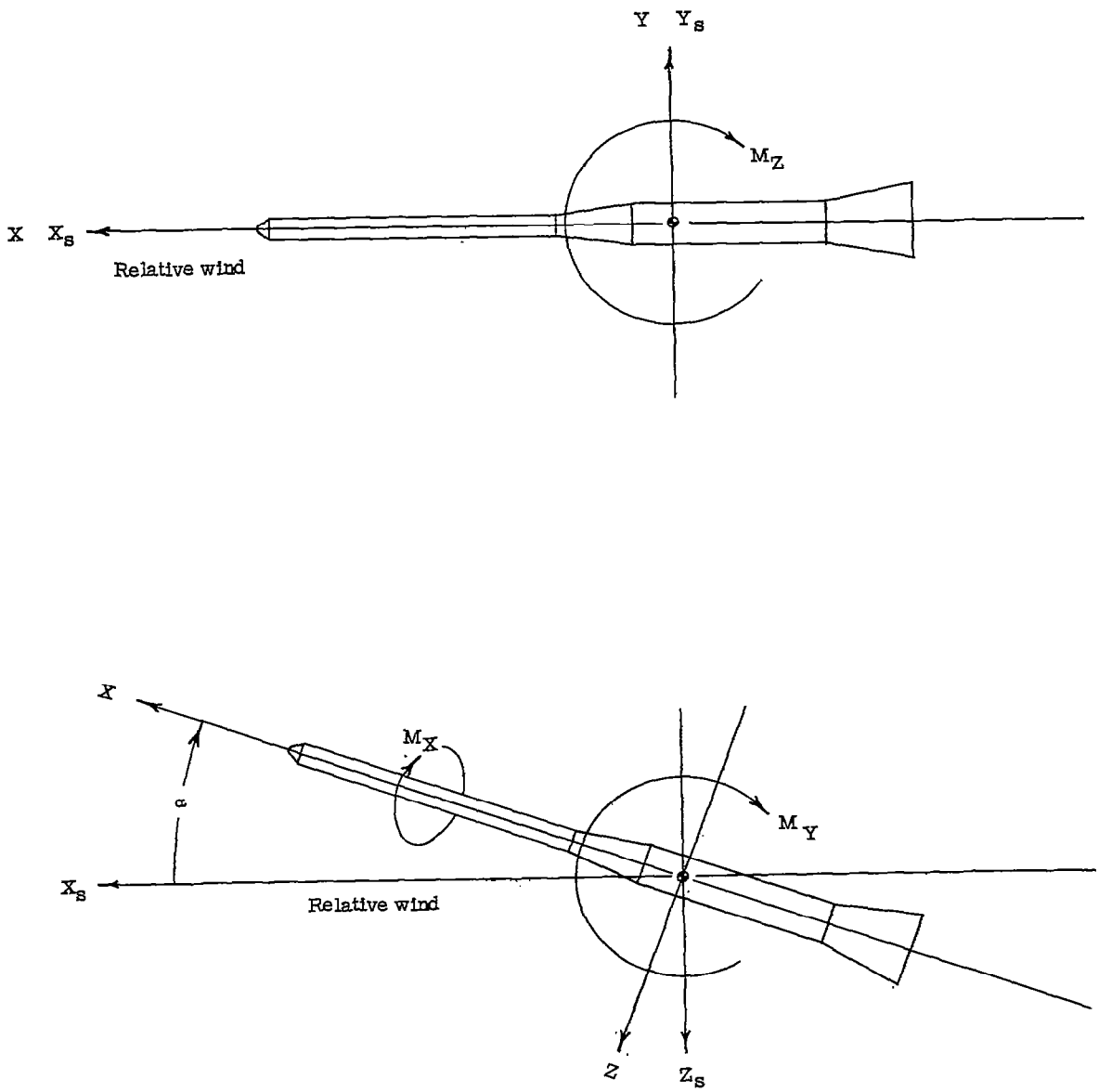

s denotes stability axis system

No subscript denotes body axis system

Figure 5.- Systems of reference axes; arrows indicate positive direction.

[redacted]

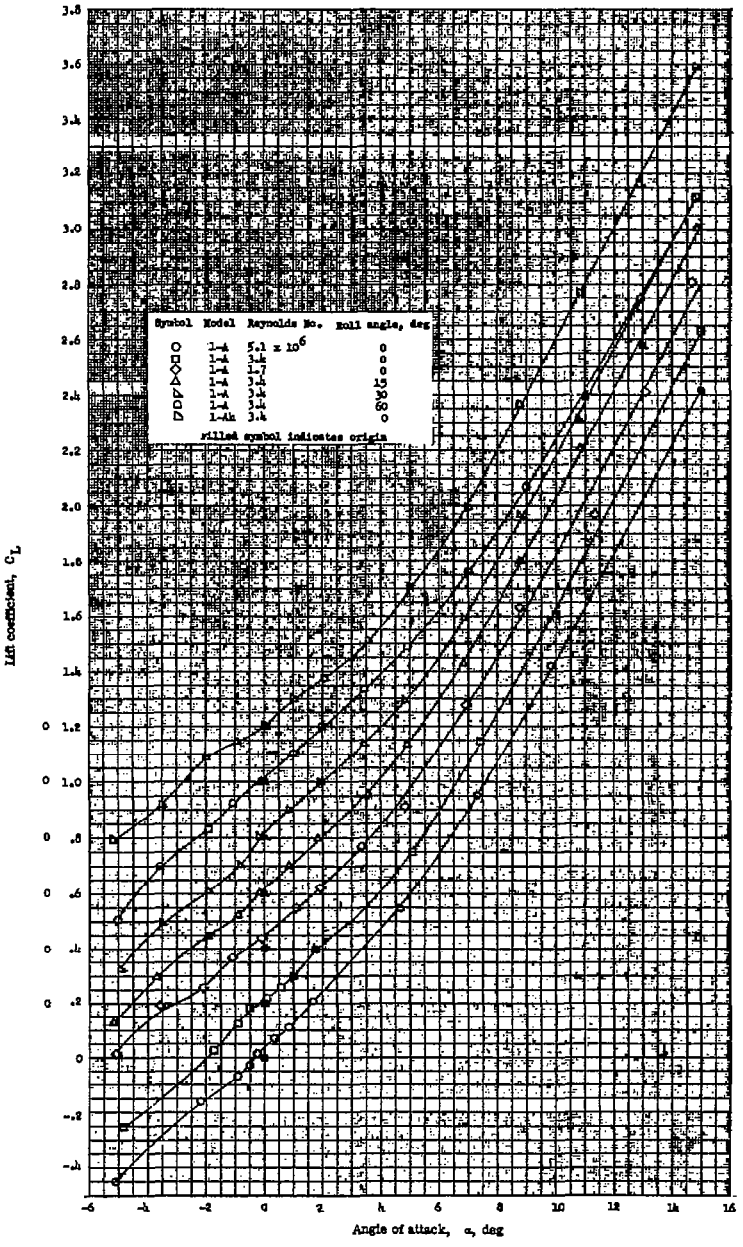

(a) Lift.

Figure 6.- Variation of the longitudinal and lateral stability parameters with angle of attack for missile configuration 1-A at various angles of roll and various Reynolds numbers and equipped with a hemispherical nose. M = 6.86.

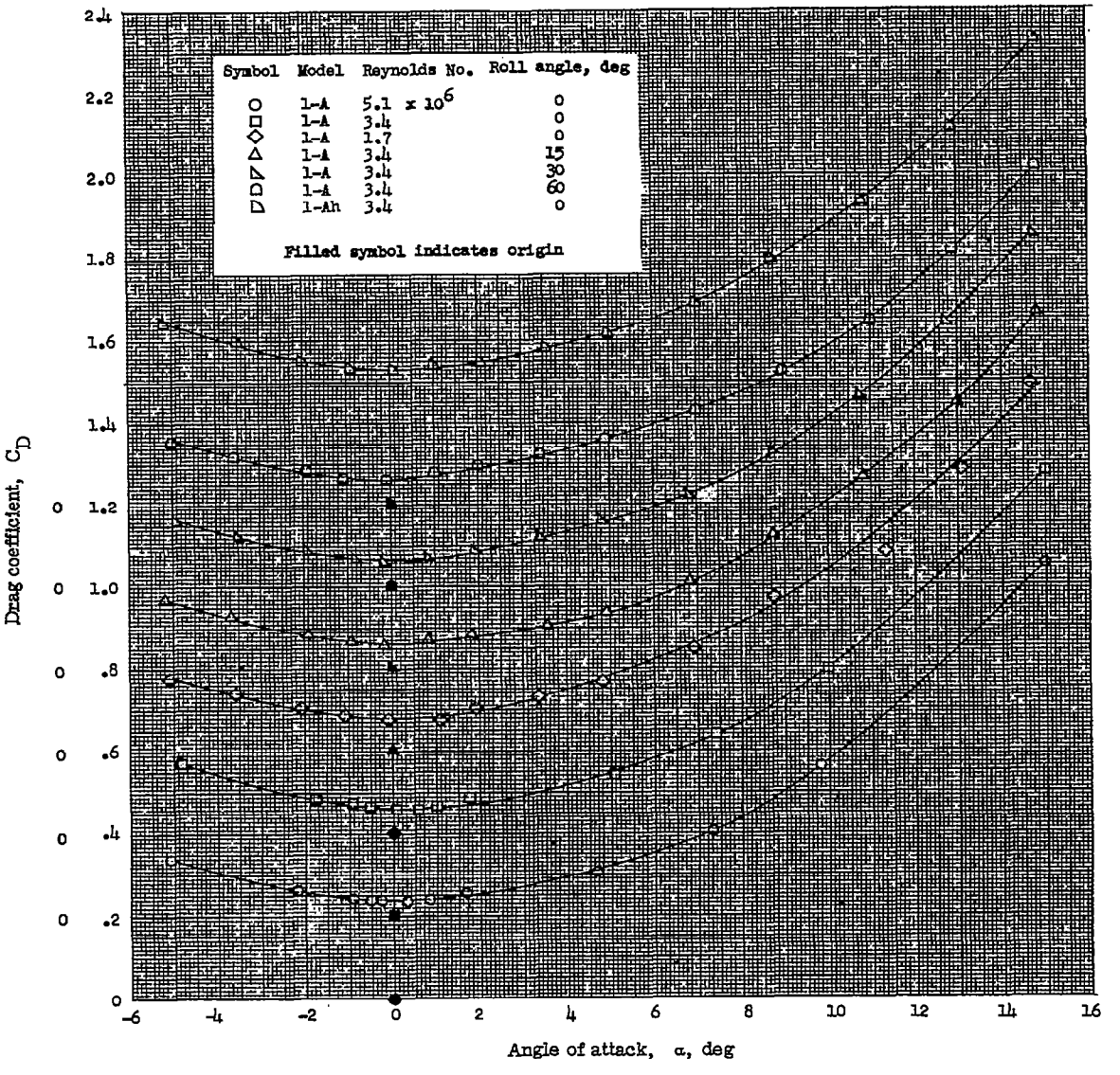

(b) Drag.

Figure 6.- Continued.

[redacted]

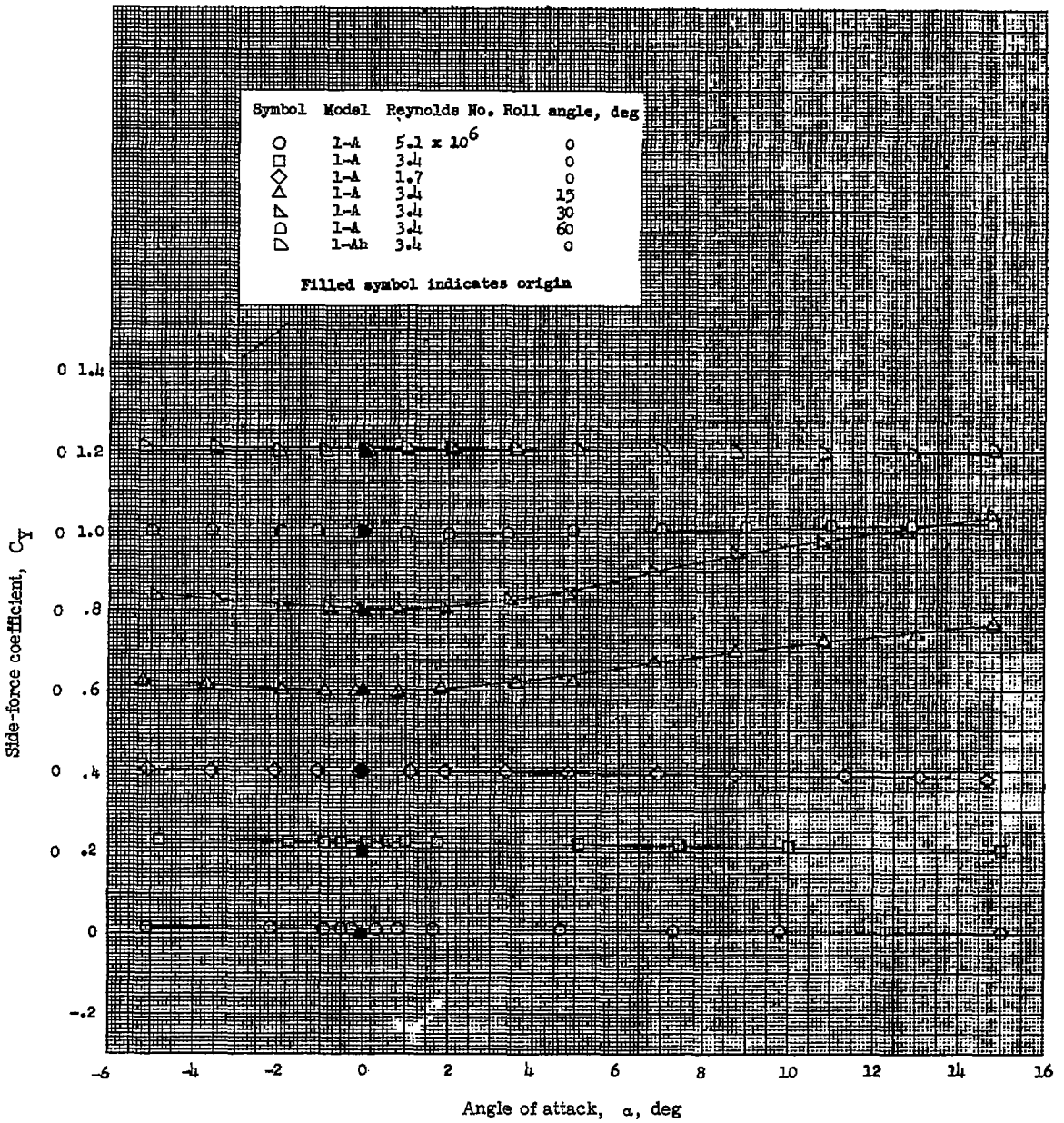

(c) Side force.

Figure 6.- Continued.

[redacted]

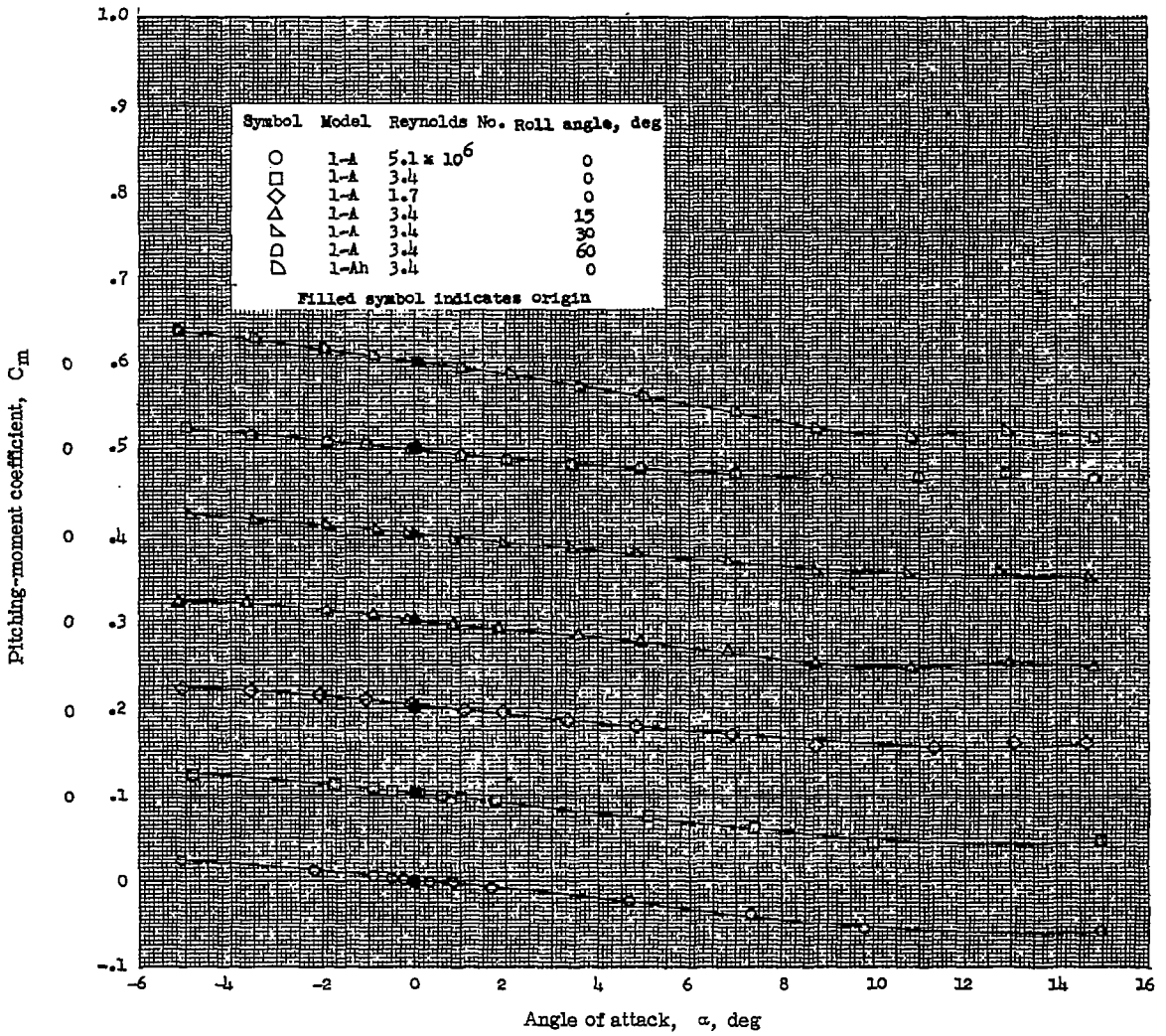

(d) Pitching moment.

Figure 6.- Continued.

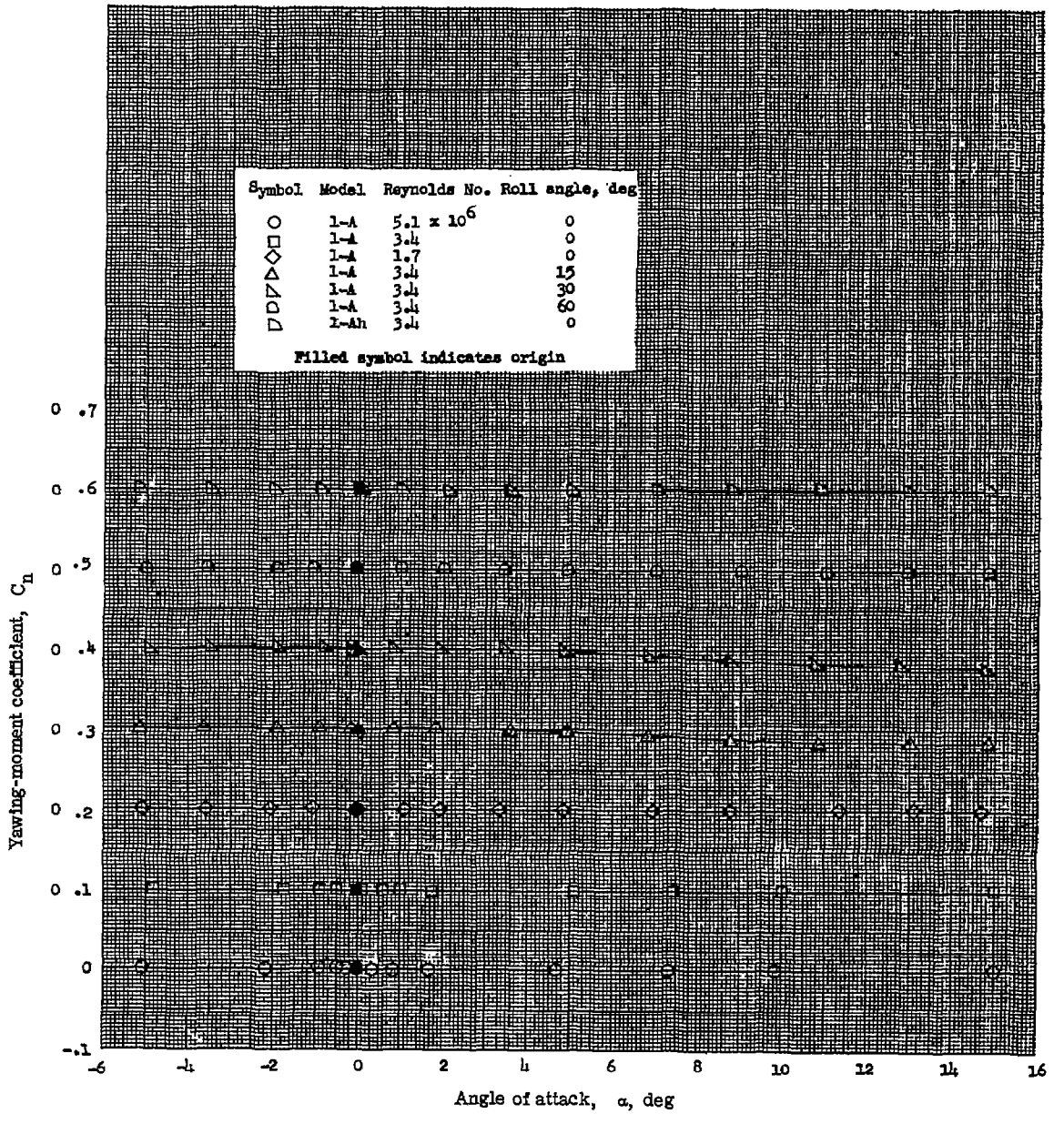

(e) Yawing moment.

Figure 6.- Continued.

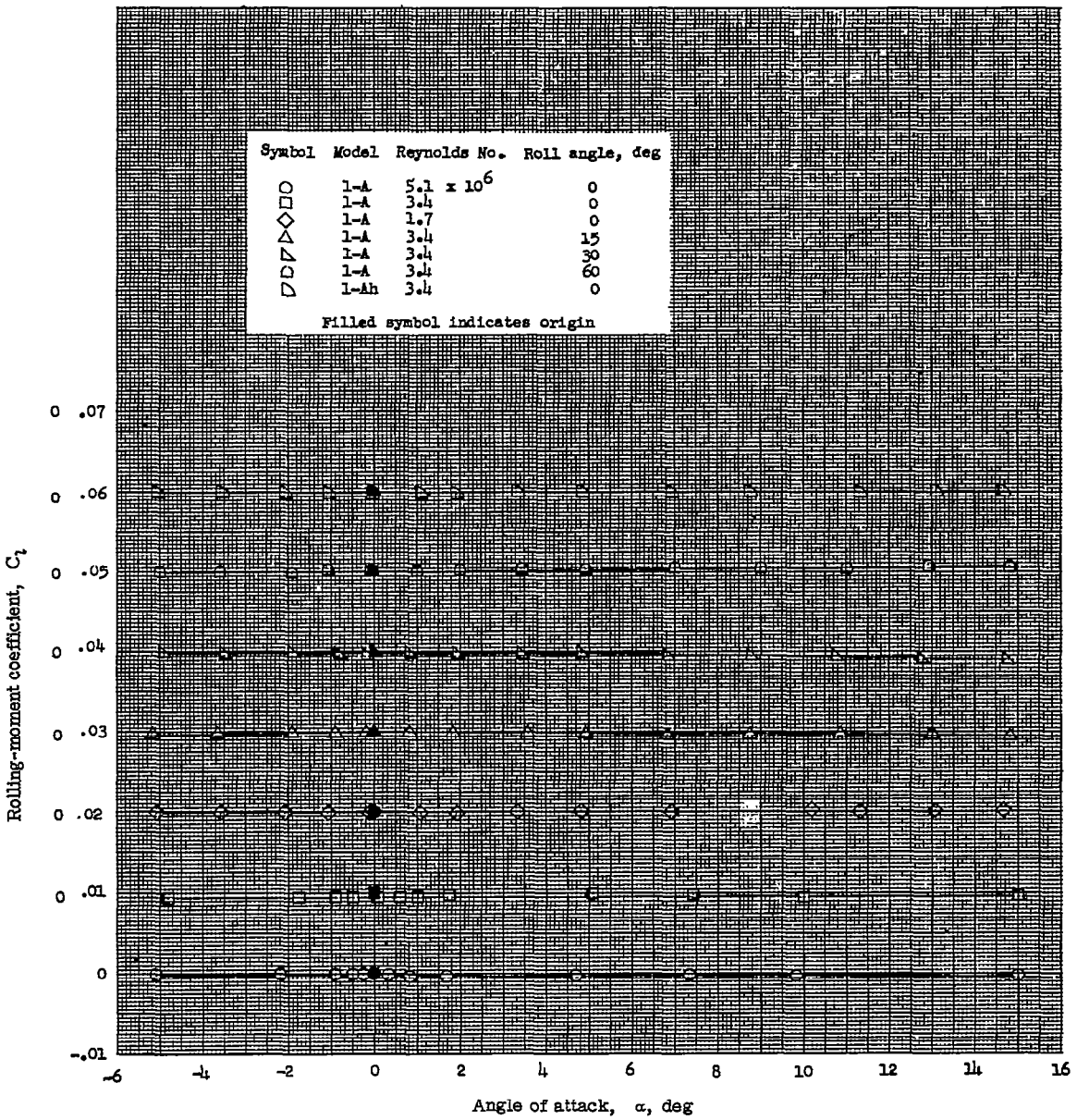

(f) Rolling moment.

Figure 6.- Continued.

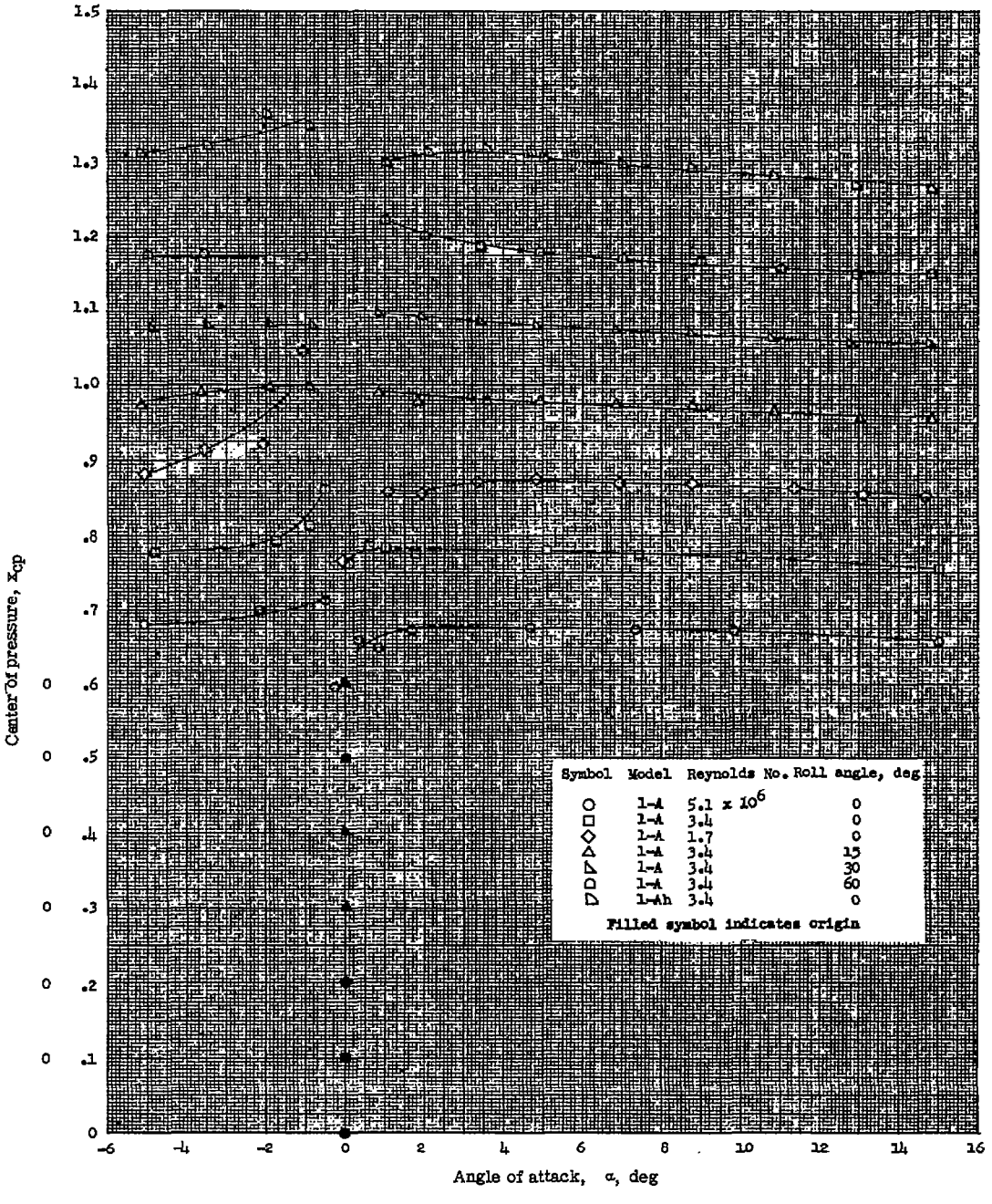

(g) Center of pressure.

Figure 6.- Continued.

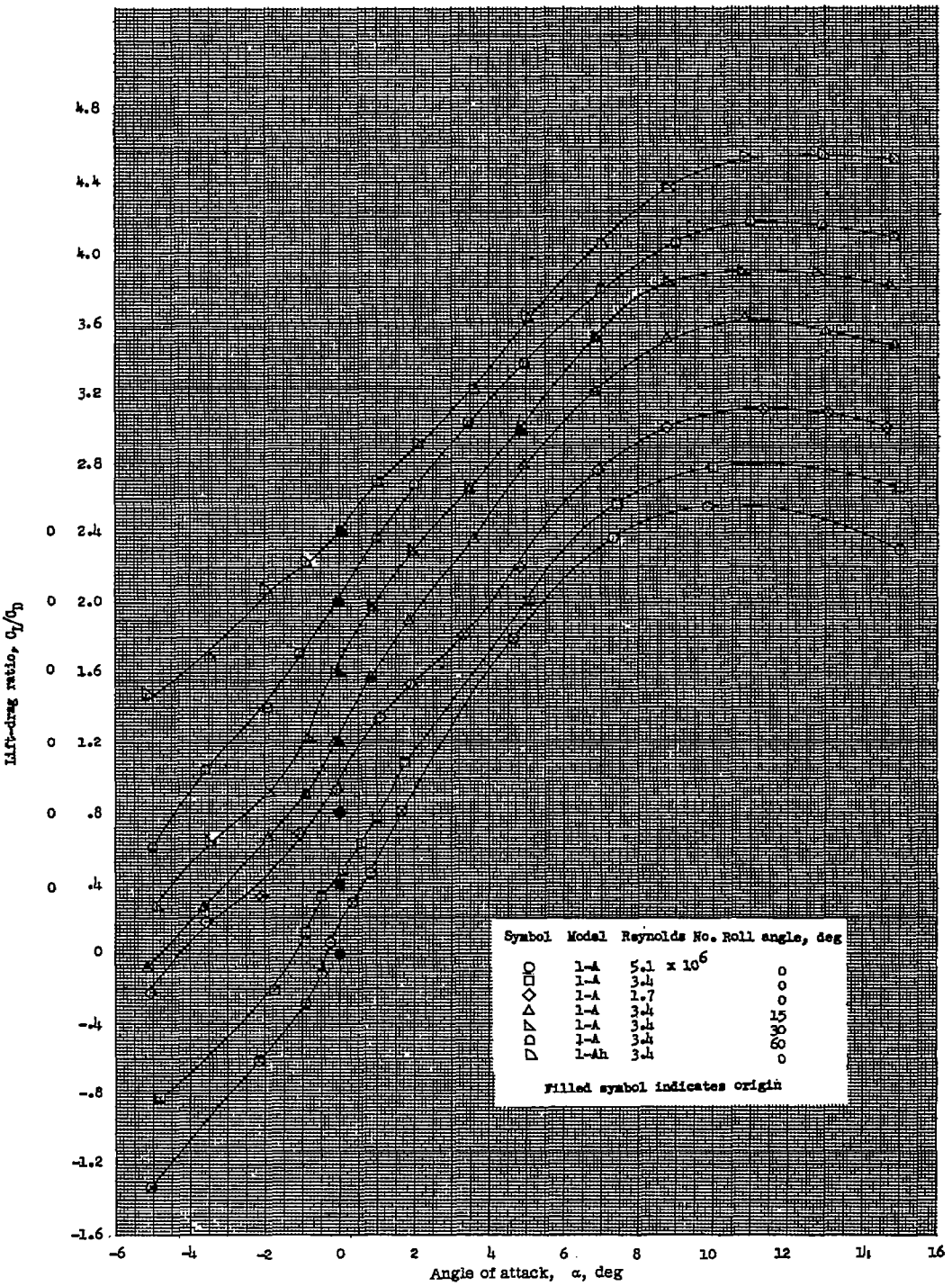

(h) Lift-drag ratio.

Figure 6.- Concluded.

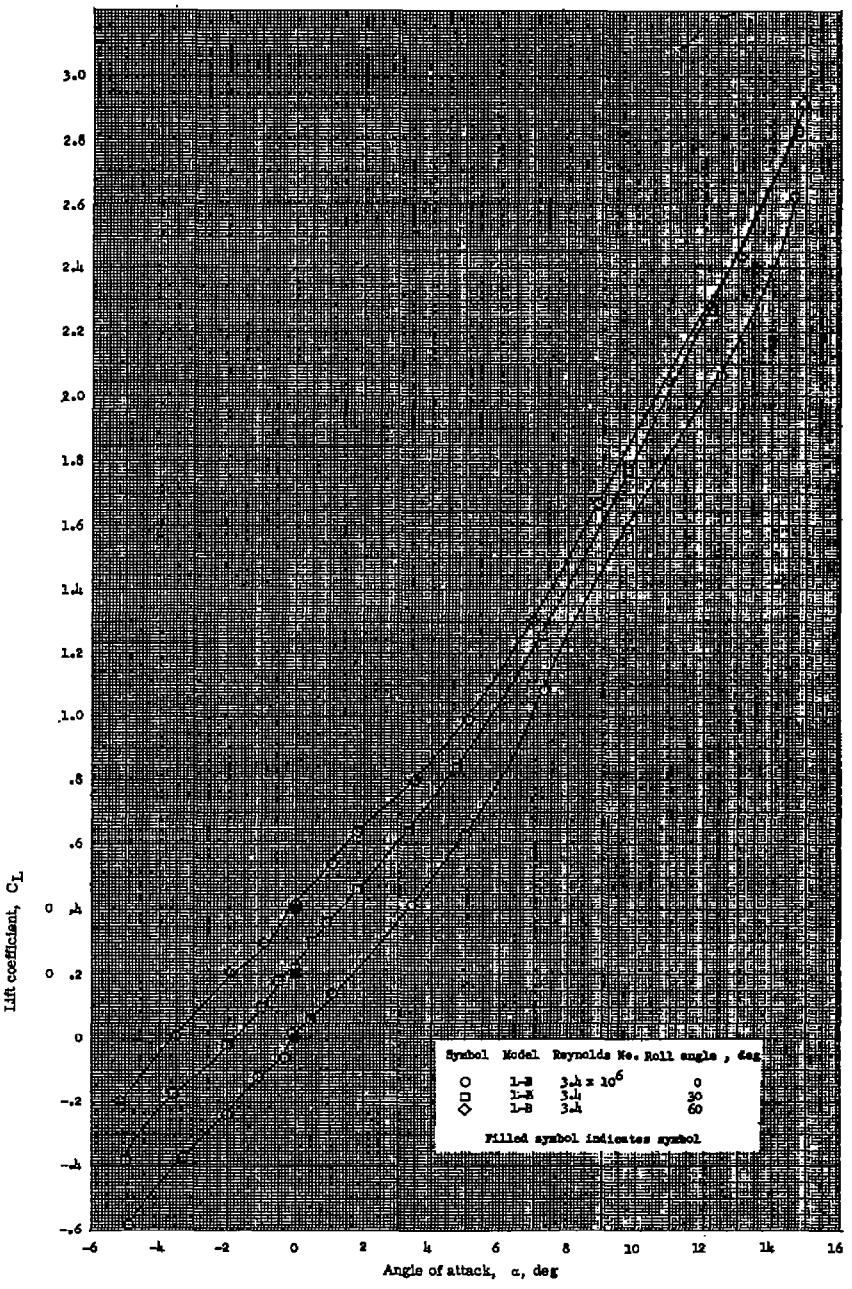

(a) Lift.

Figure 7.- Variation of the longitudinal and lateral stability parameters with angle of attack for configuration 1-B at various angles of roll. M = 6.86.

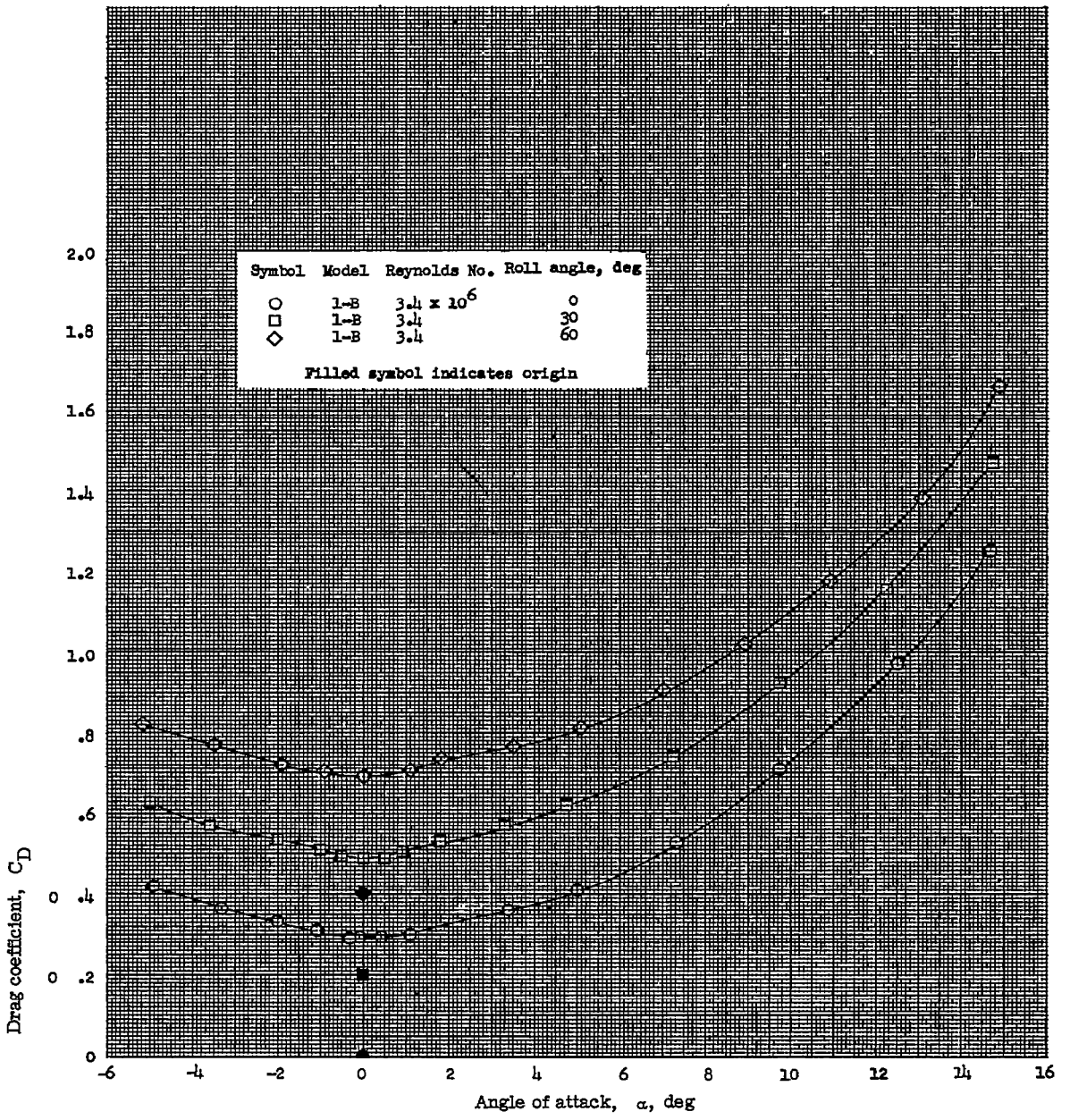

(b) Drag.

Figure 7.- Continued.

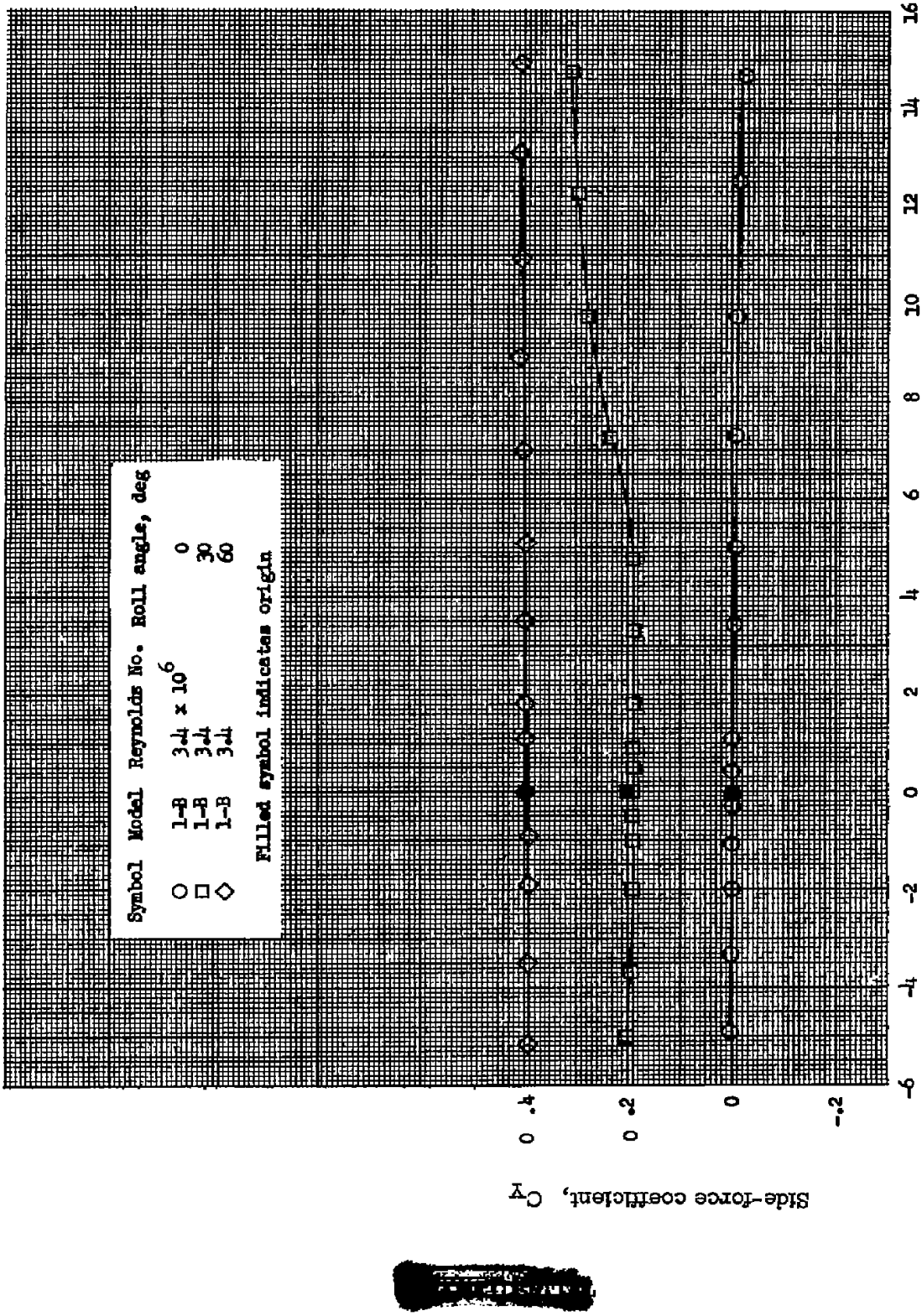

(c) Side force.

Figure 7.- Continued.

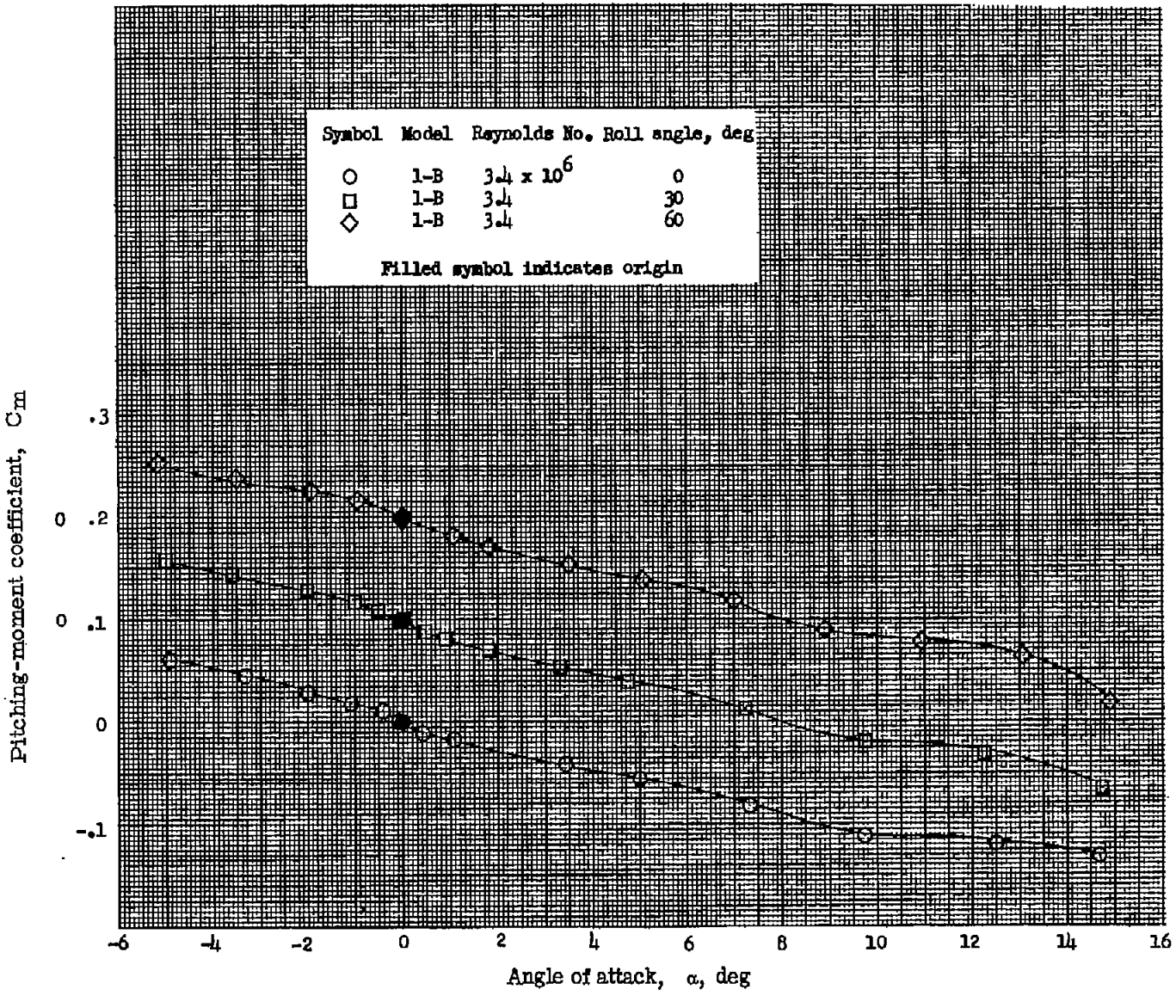

(d) Pitching moment.

Figure 7.- Continued.

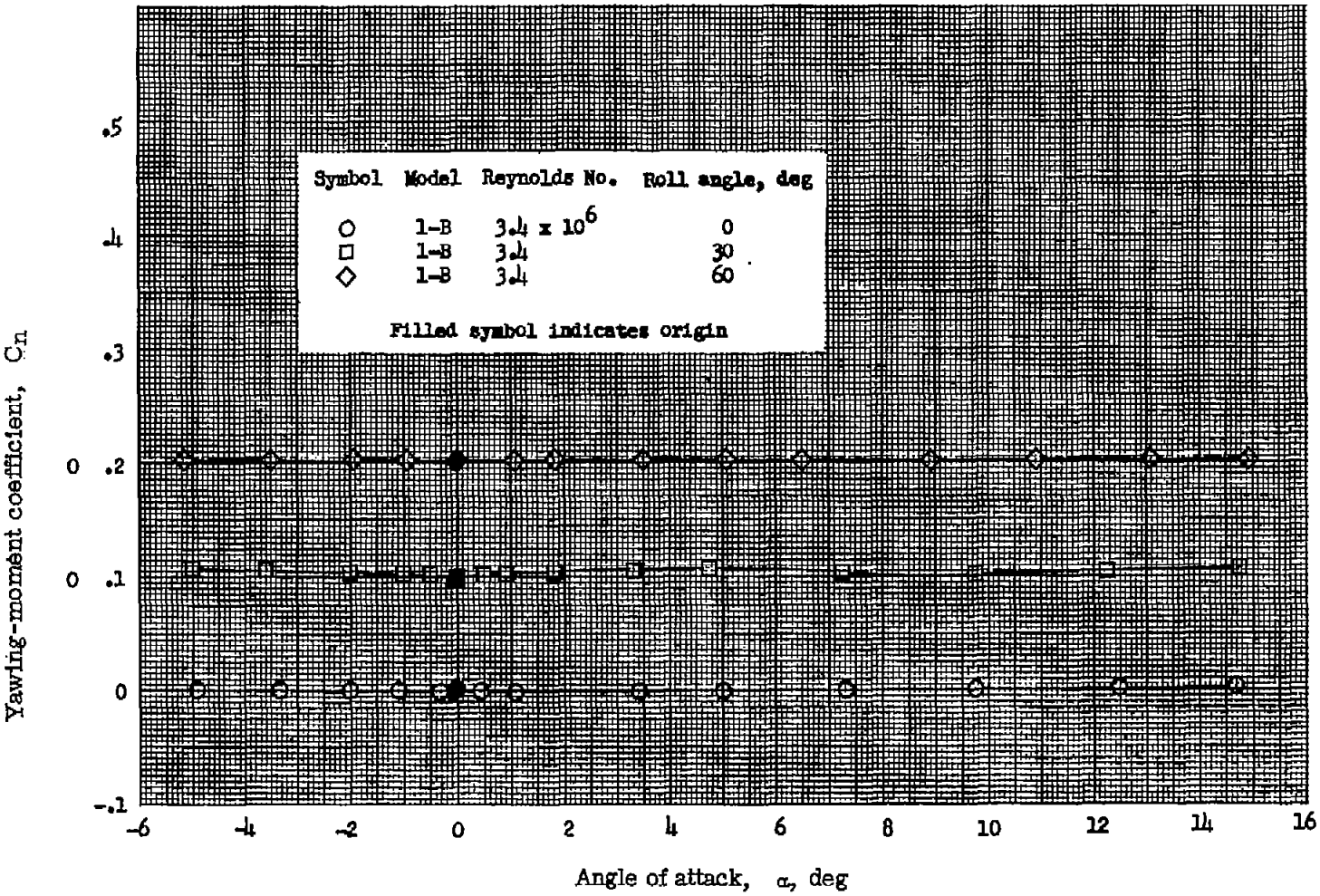

(e) Yawing moment.

Figure 7.- Continued.

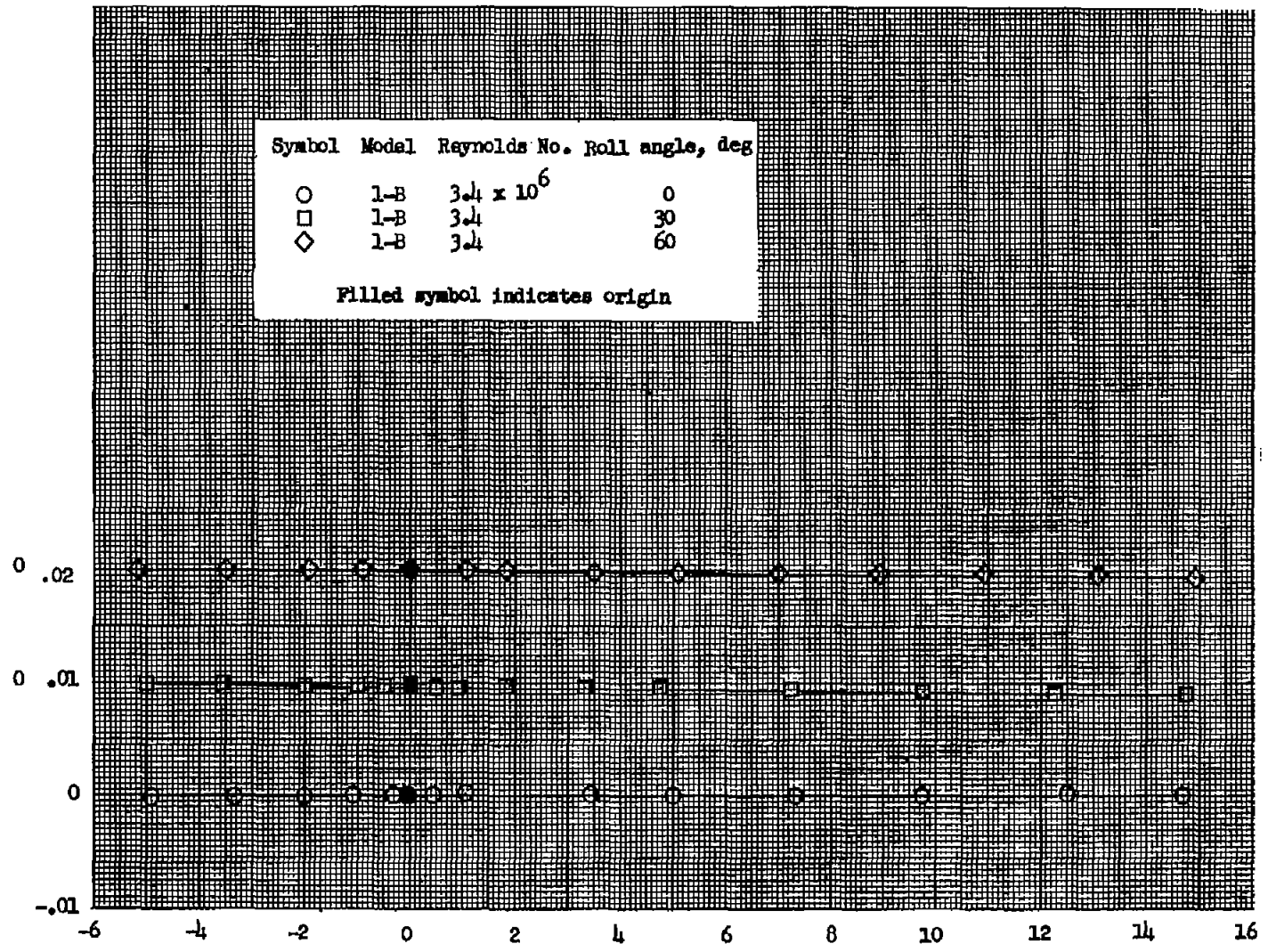

(f) Rolling moment.

Figure 7.- Continued.

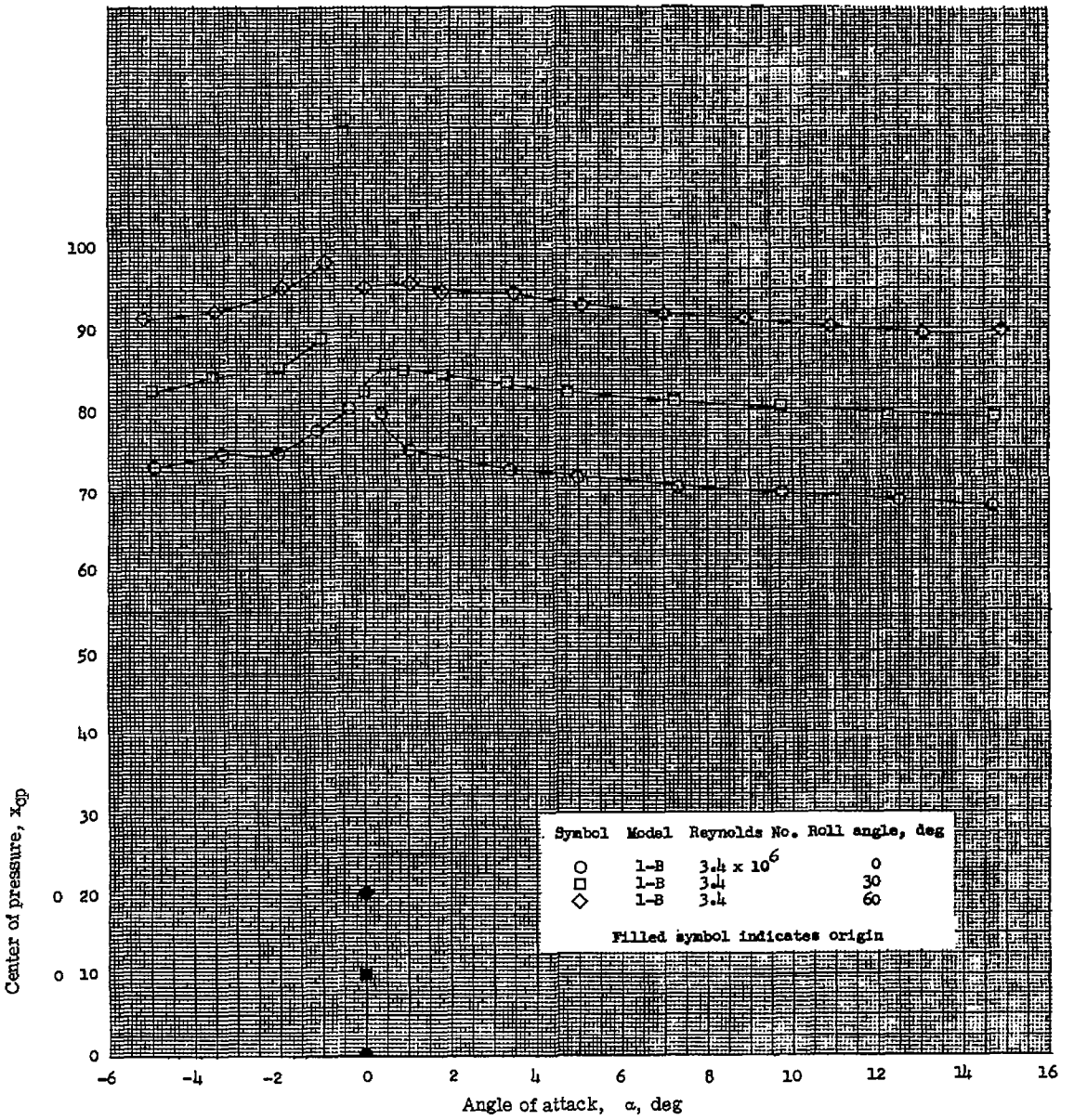

(g) Center of pressure.

Figure 7.- Continued.

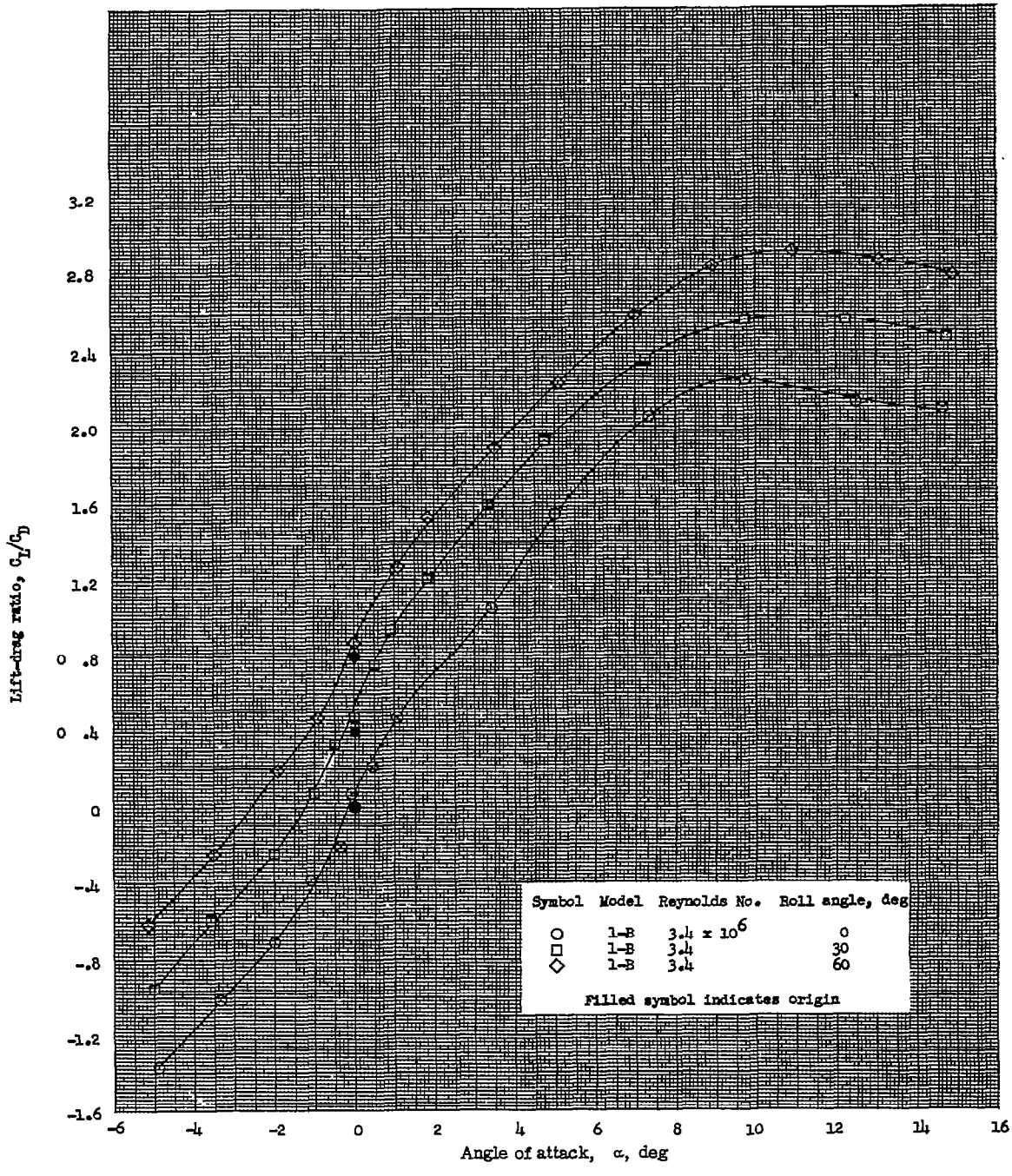

(h) Lift-drag ratio.

Figure 7.- Concluded.

[redacted]

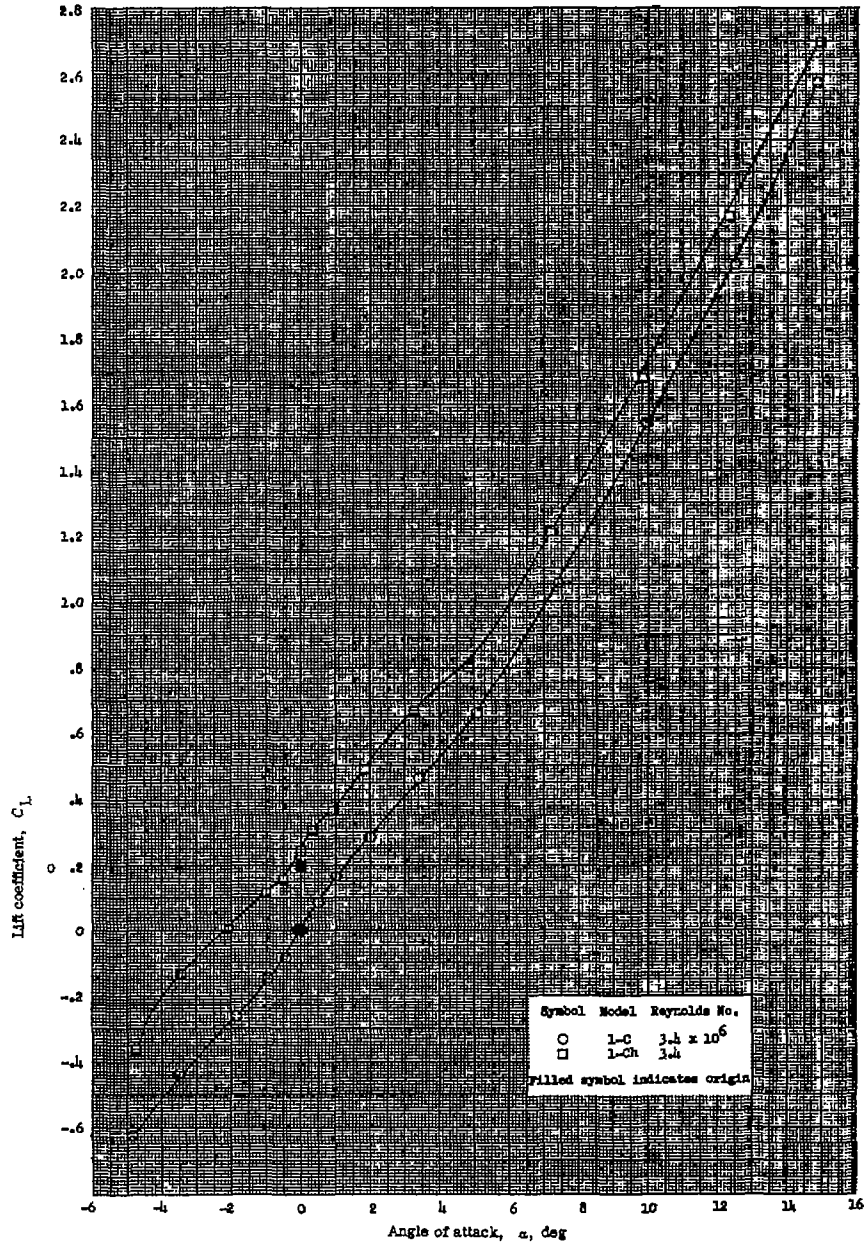

(a) Lift.

Figure 8.- Variation of the longitudinal stability parameters with angle of attack for configuration 1-C with and without hemispherical nose. M = 6.86.

[redacted]

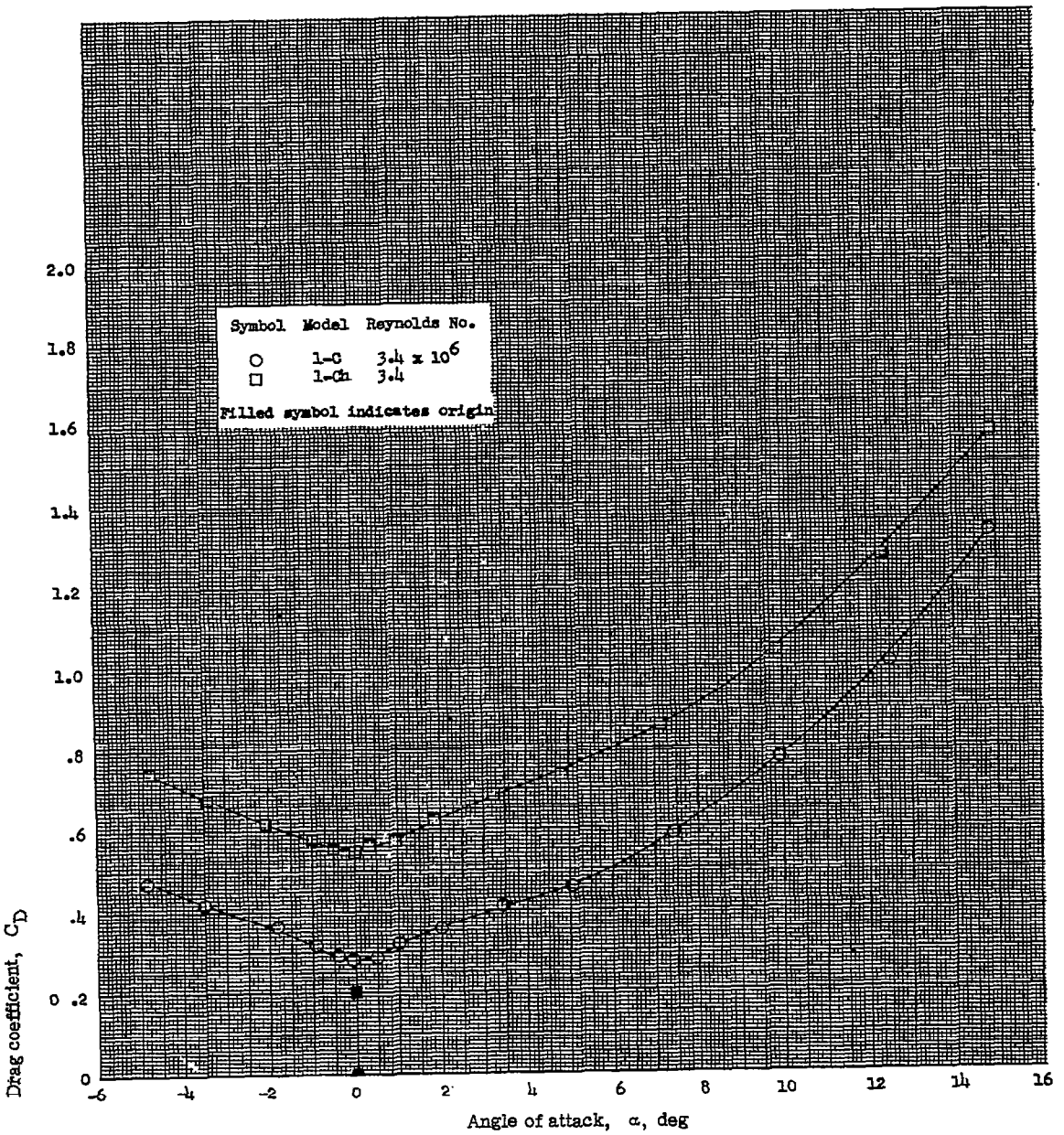

(b) Drag.

Figure 8.- Continued.

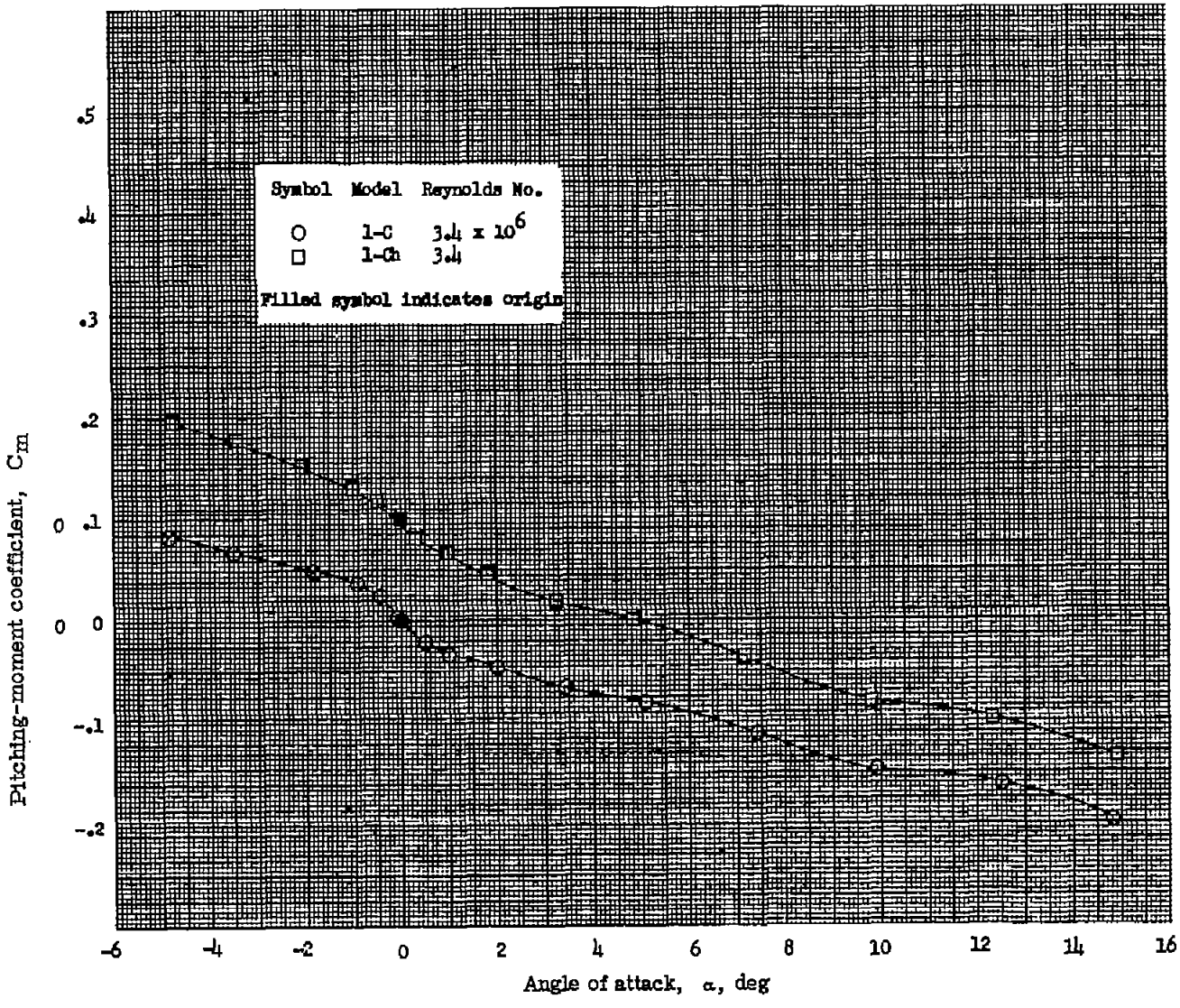

(c) Pitching moment.

Figure 8.- Continued.

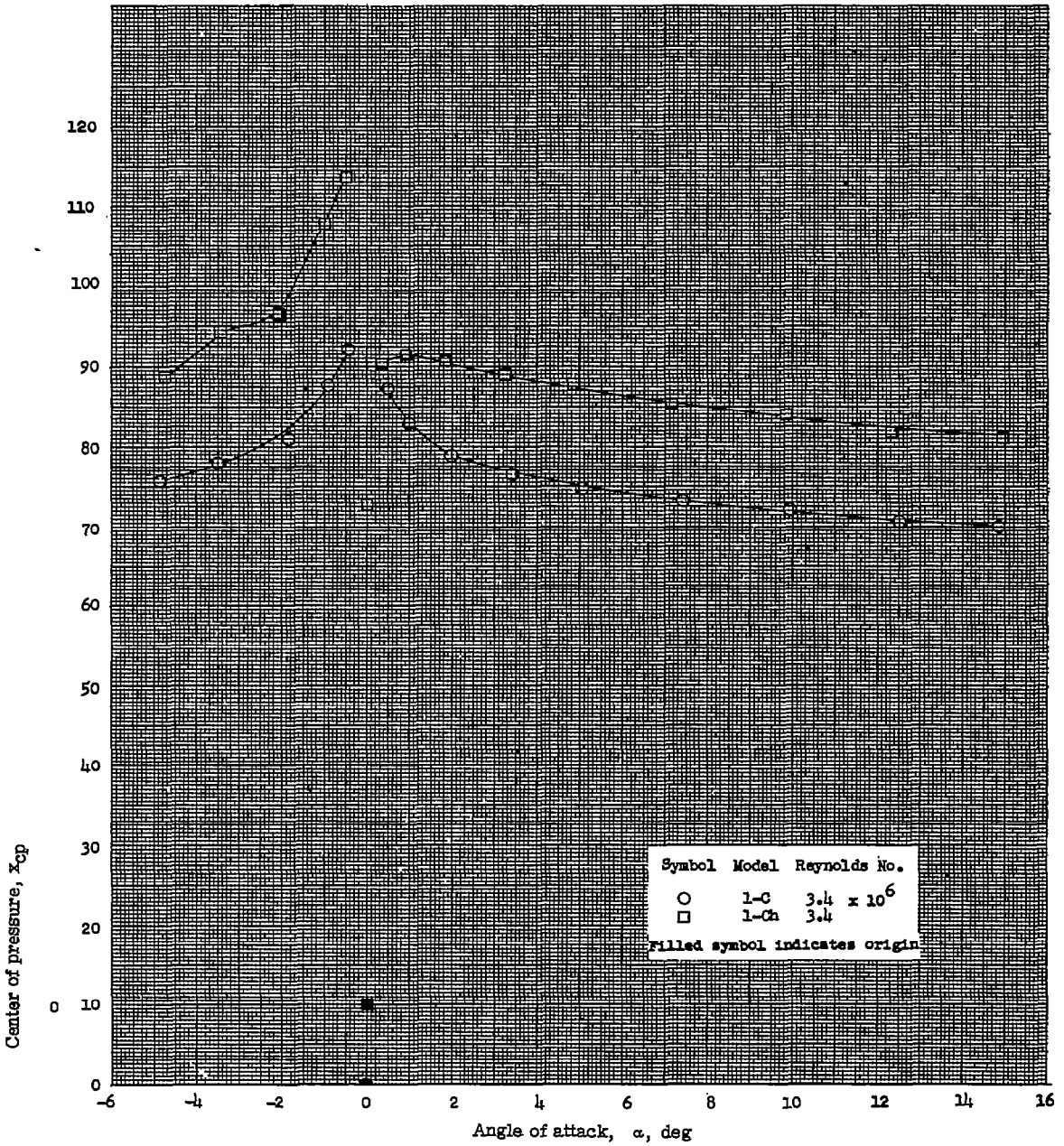

(d) Center of pressure.

Figure 8.- Continued.

[redacted]

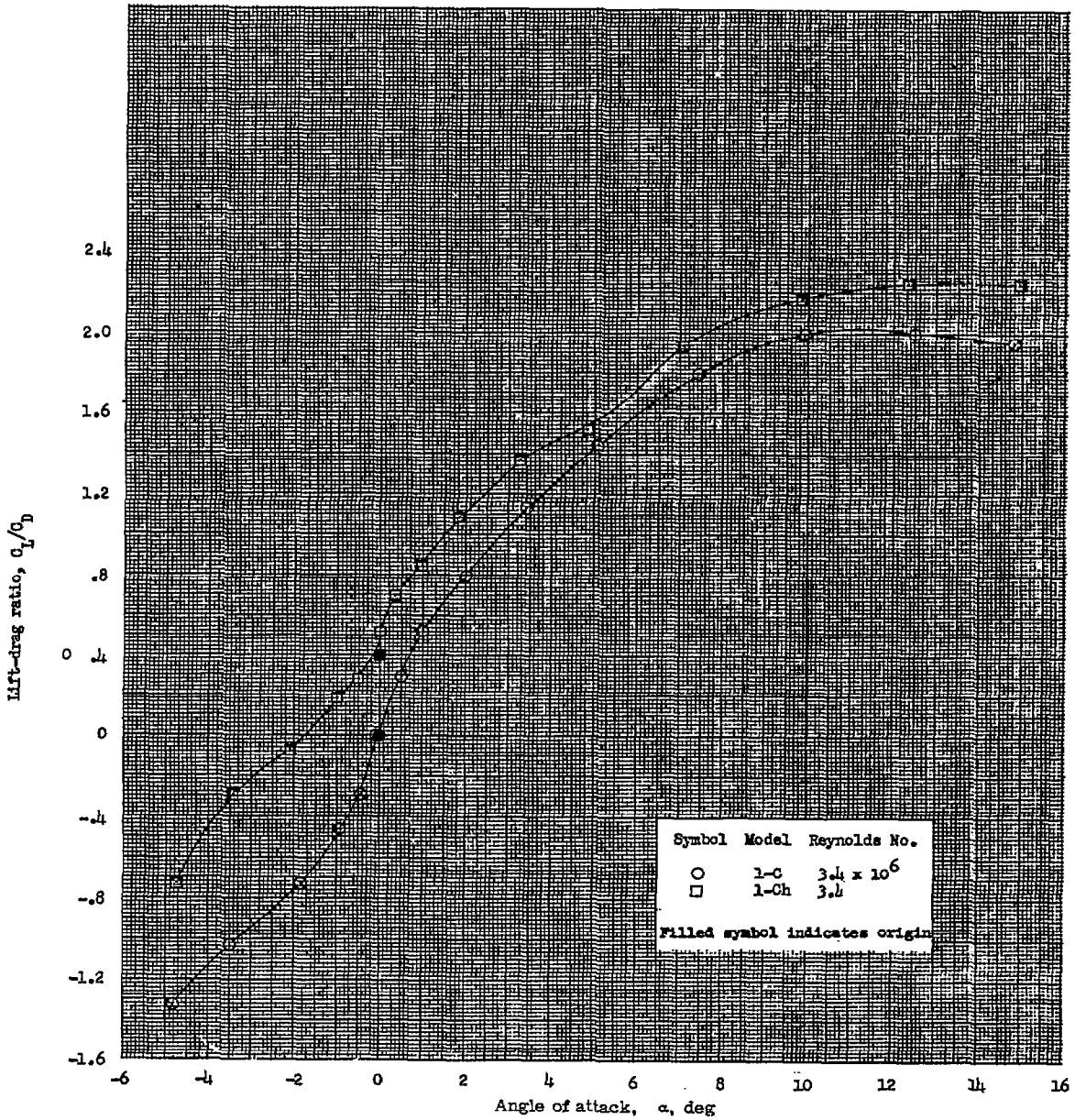

(e) Lift-drag ratio.

Figure 8.- Concluded.

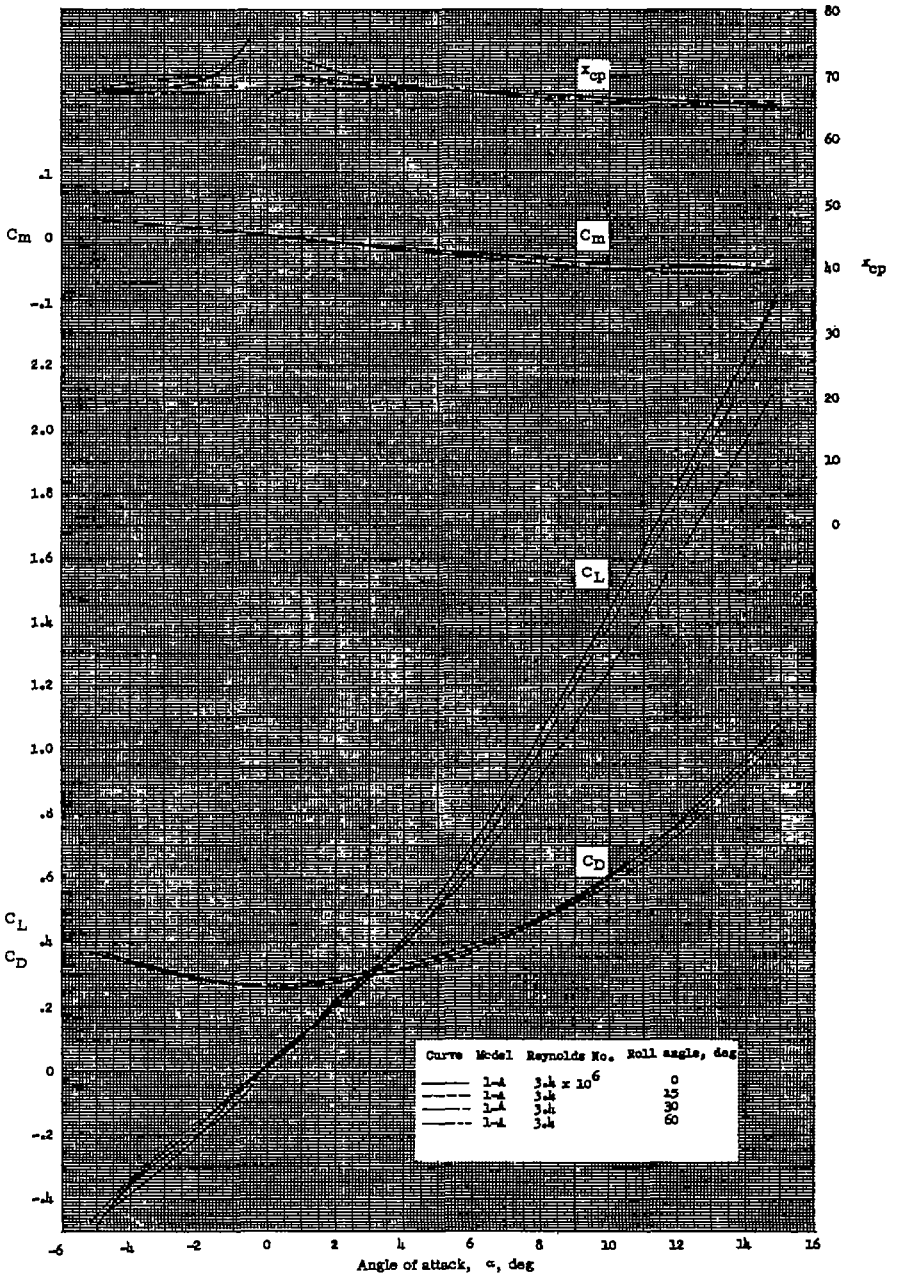

(a) Lift, drag, pitch, and center of pressure.

Figure 9.- Comparison of the longitudinal characteristics of configuration 1-A for various angles of roll. M = 6.86.

[redacted]

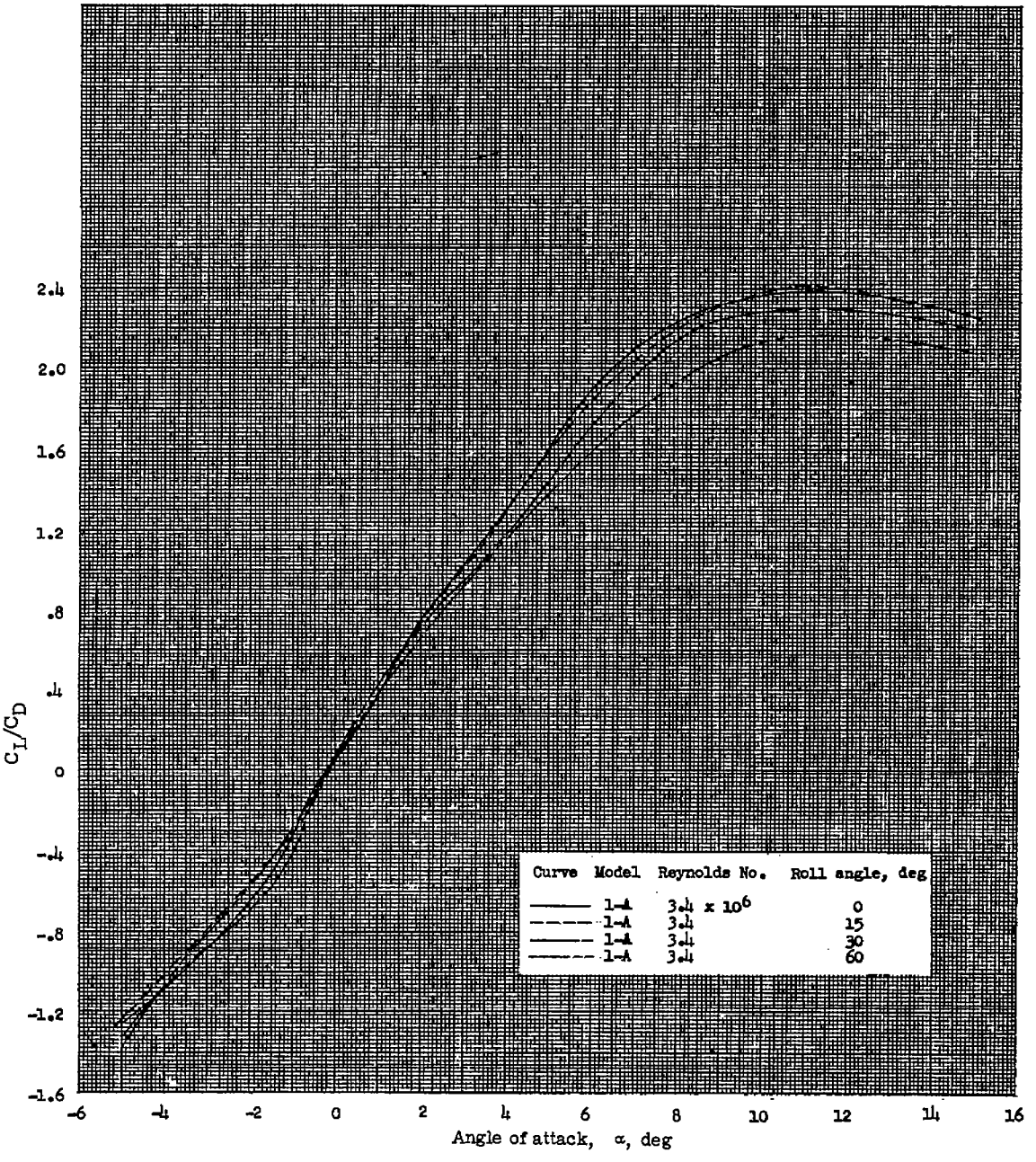

(b) Lift-drag ratio.

Figure 9.- Concluded.

[redacted]

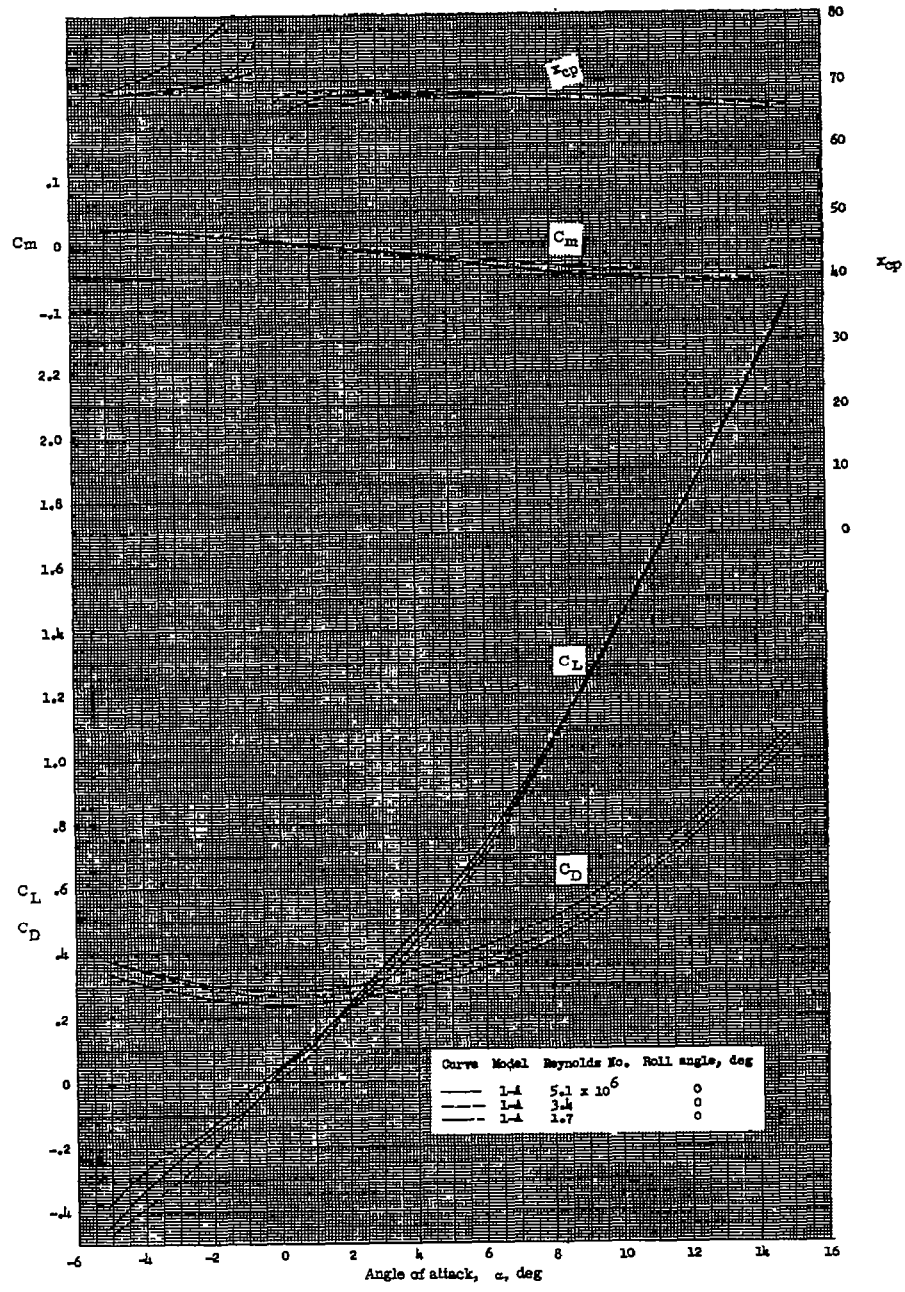

(a) Lift, drag, pitch, and center of pressure.

Figure 10.- Comparison of the longitudinal characteristics of configuration 1-A for various Reynolds numbers. M = 6.86.

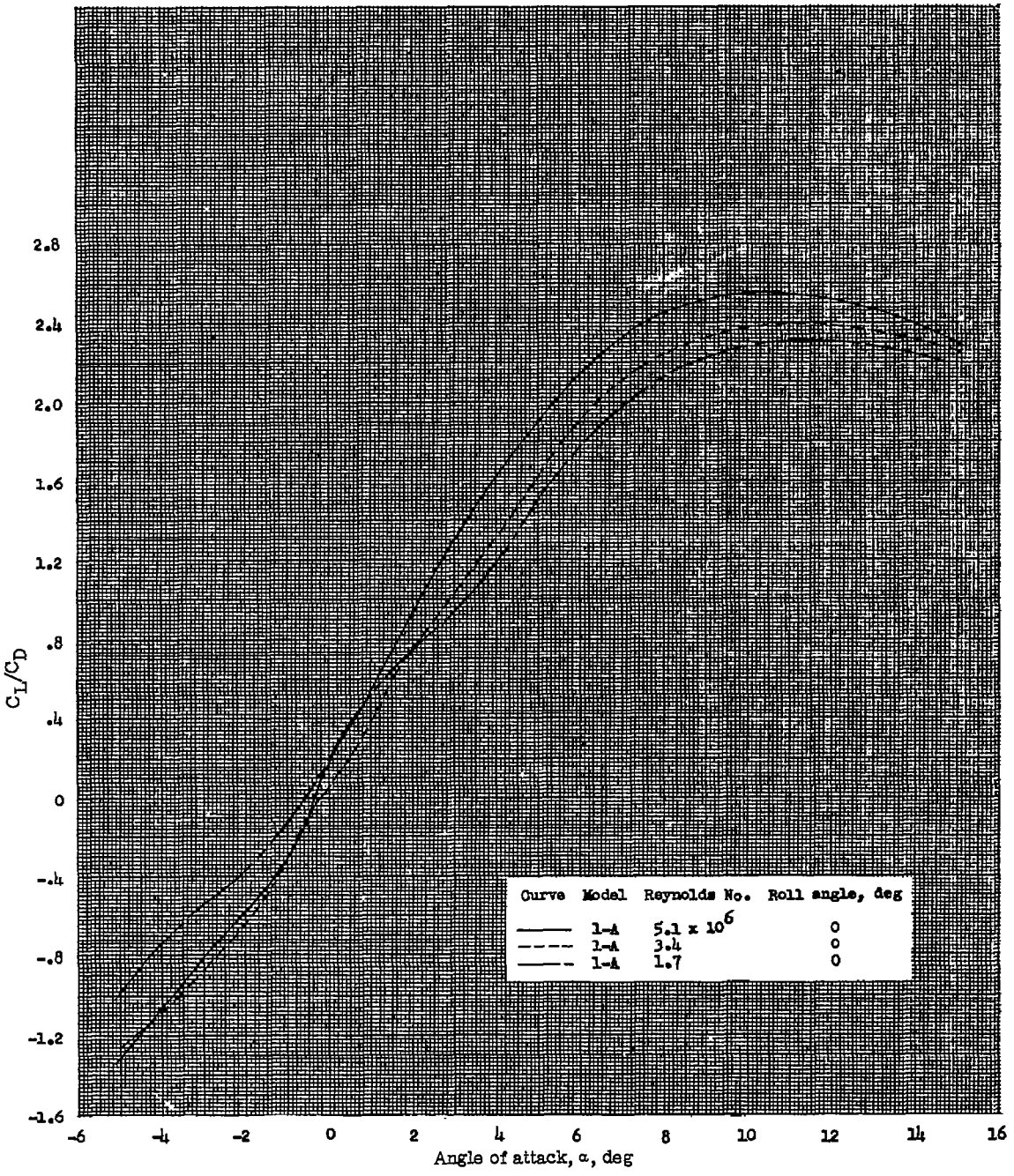

(b) Lift-drag ratio.

Figure 10.- Concluded.

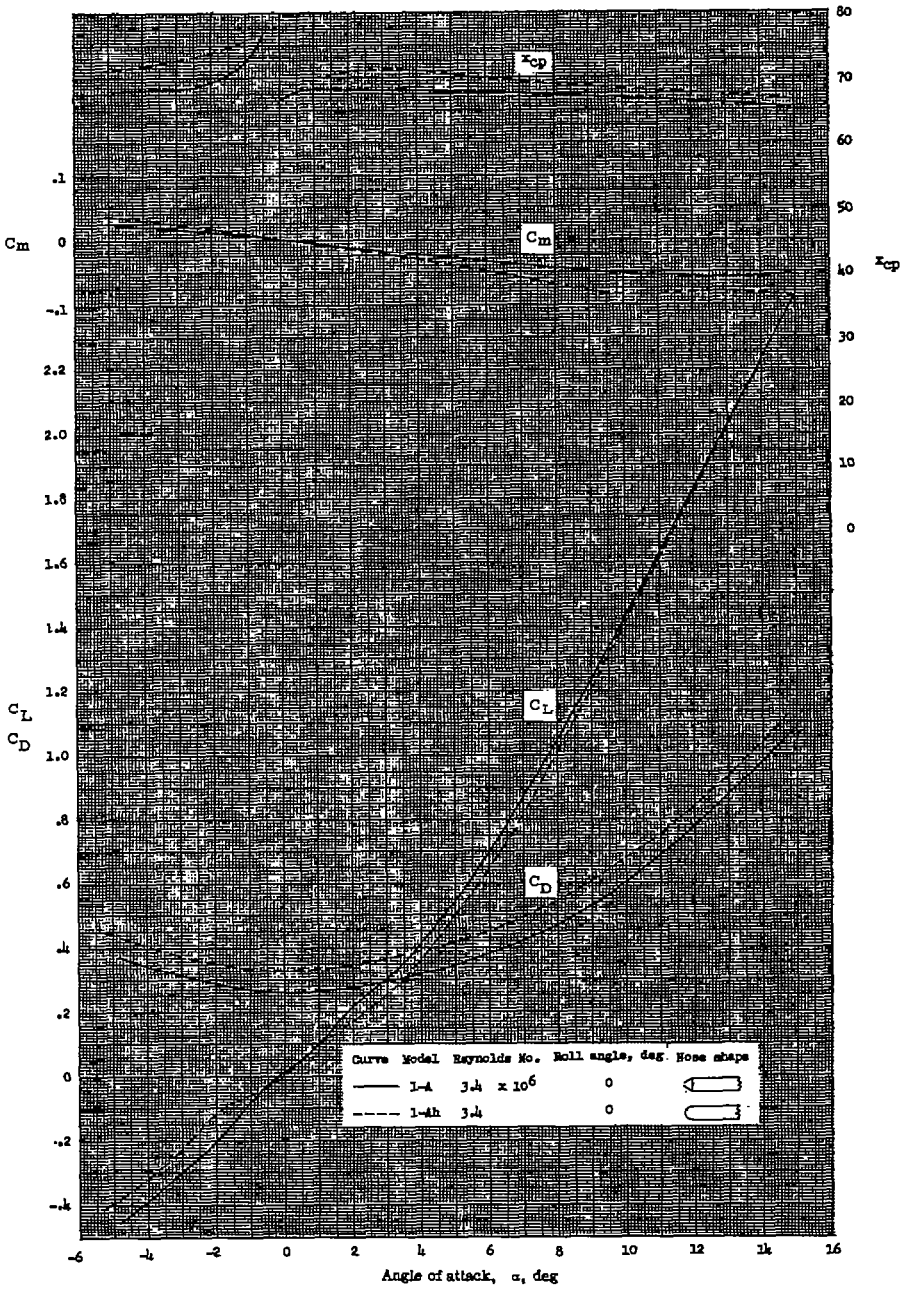

(a) Lift, drag, pitch, and center of pressure.

Figure 11.- Comparison of the longitudinal characteristics of configuration 1-A with and without hemispherical nose. M = 6.86.

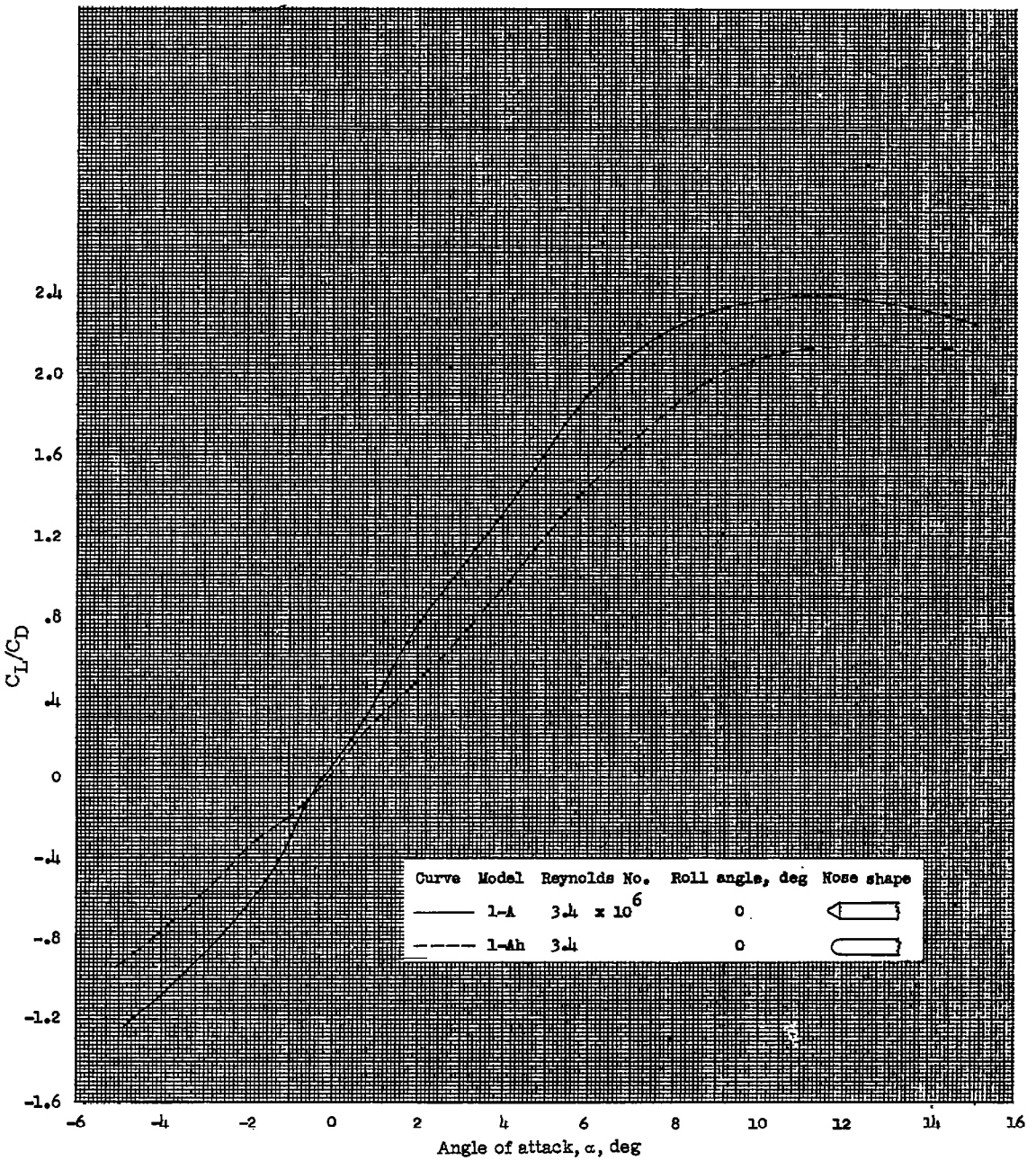

(b) Lift-drag ratio.

Figure 11.- Concluded.

[redacted]

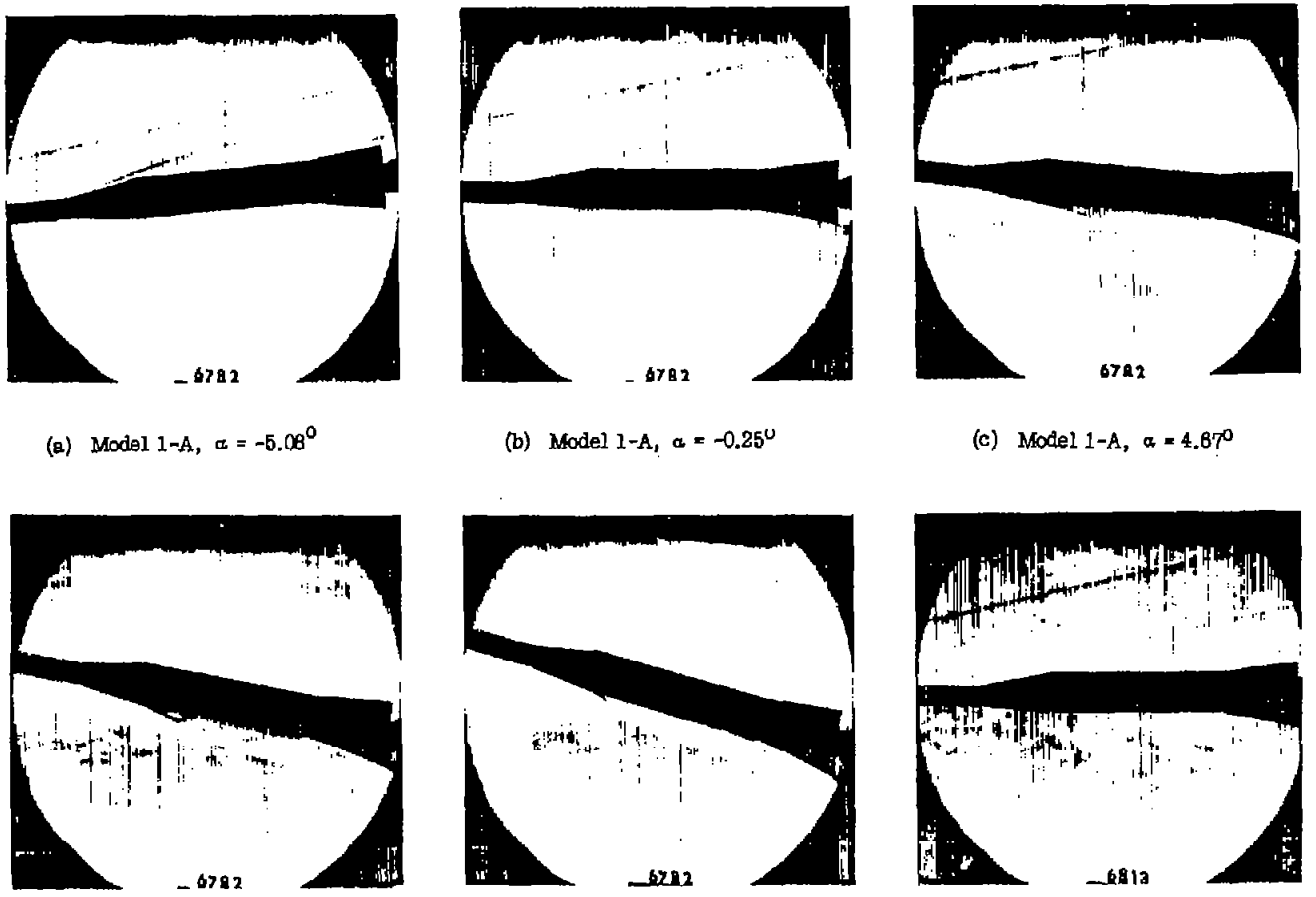

(a) Model 1-A, $\alpha = -5.08^{\circ}$ (b) Model 1-A, $\alpha = -0.25^{\circ}$ (c) Model 1-A, $\alpha = 4.87^{\circ}$

(d) Model 1-A, $\alpha = 9.83^{\circ}$ (e) Model 1-A, $\alpha = 15.00^{\circ}$ (f) Model 1-Ah, $\alpha = 0.08^{\circ}$

L-57-189

Figure 12.- Schlieren photographs of model 1-A at various angles of attack and model $1\text{-}A_h$. M = 6.86; roll angle, 0°; R, 3.4×10^6.

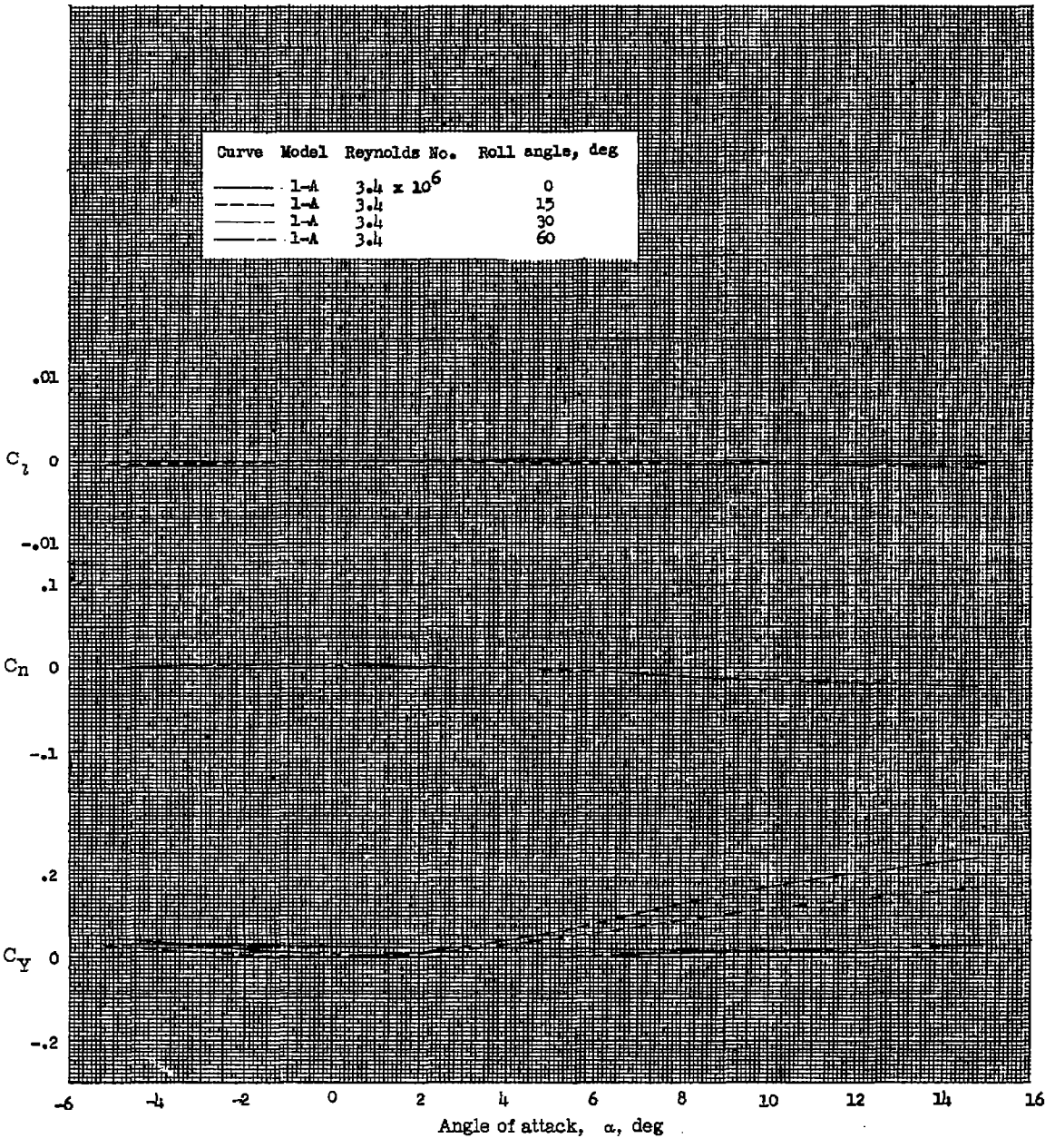

Figure 13.- Comparison of the lateral characteristics of configuration 1-A for various angles of roll. M = 6.86.

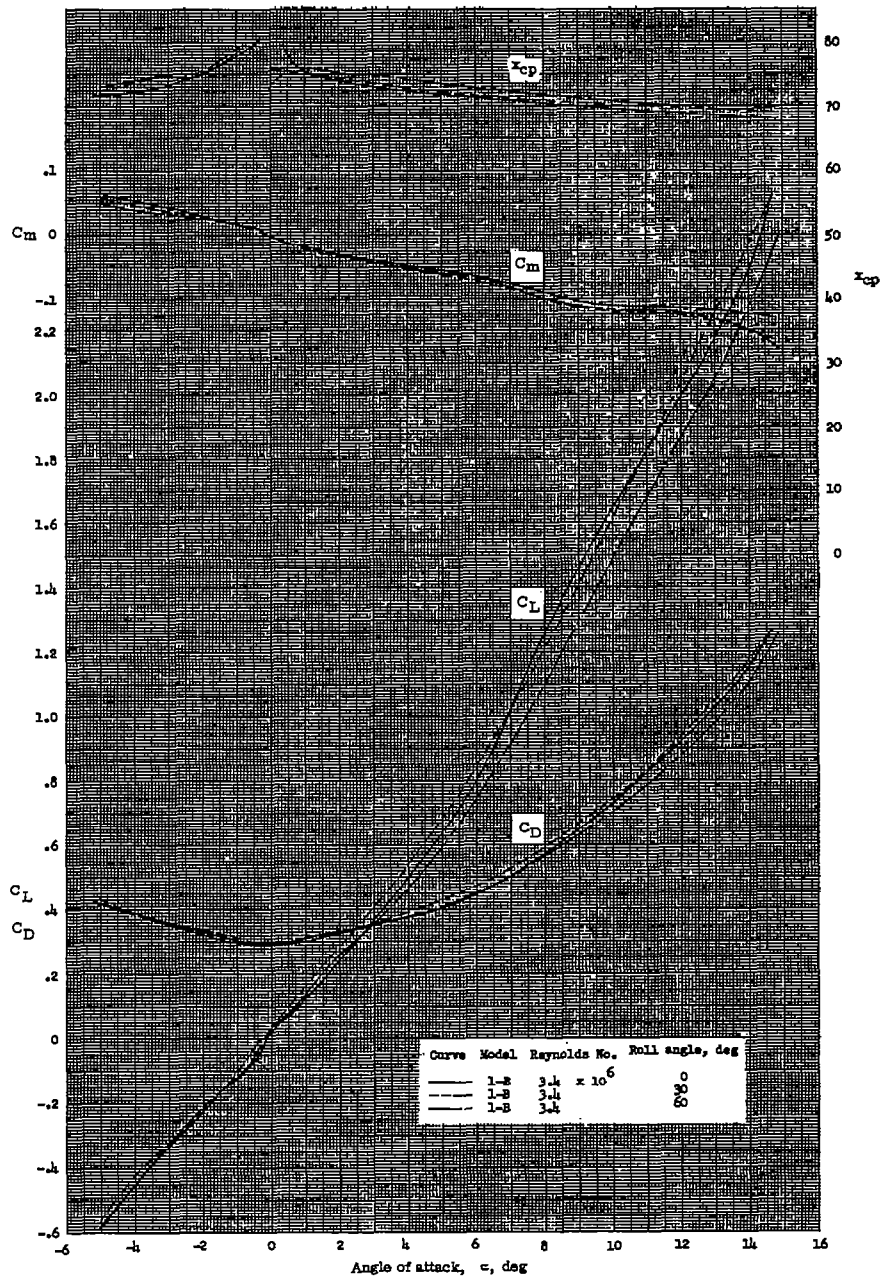

(a) Lift, drag, pitch, and center of pressure.

Figure 14.- Comparison of the longitudinal characteristics of configuration 1-B for various angles of roll. M = 6.86.

[redacted]

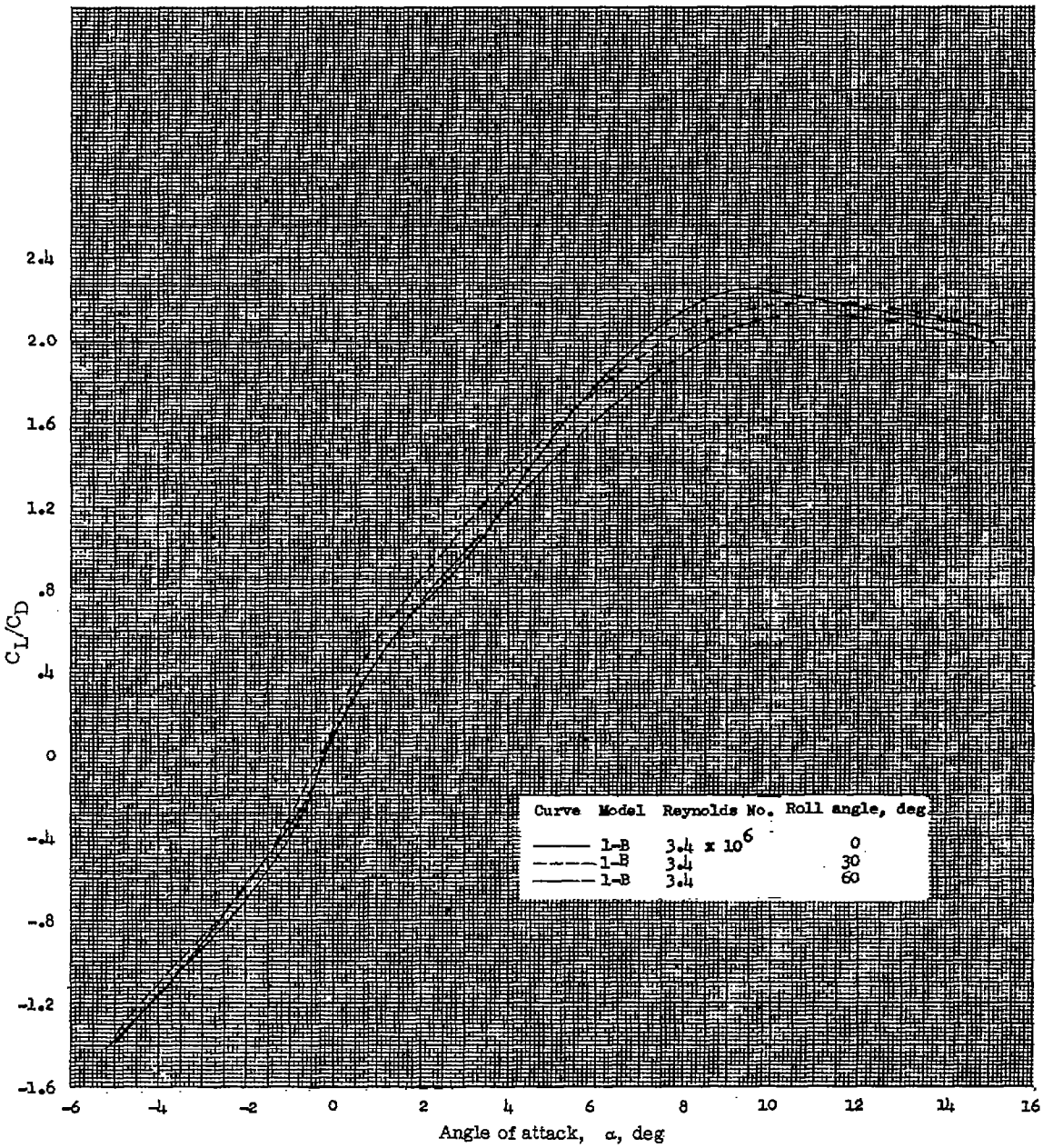

(b) Lift-drag ratio.

Figure 14.- Concluded.

[redacted]

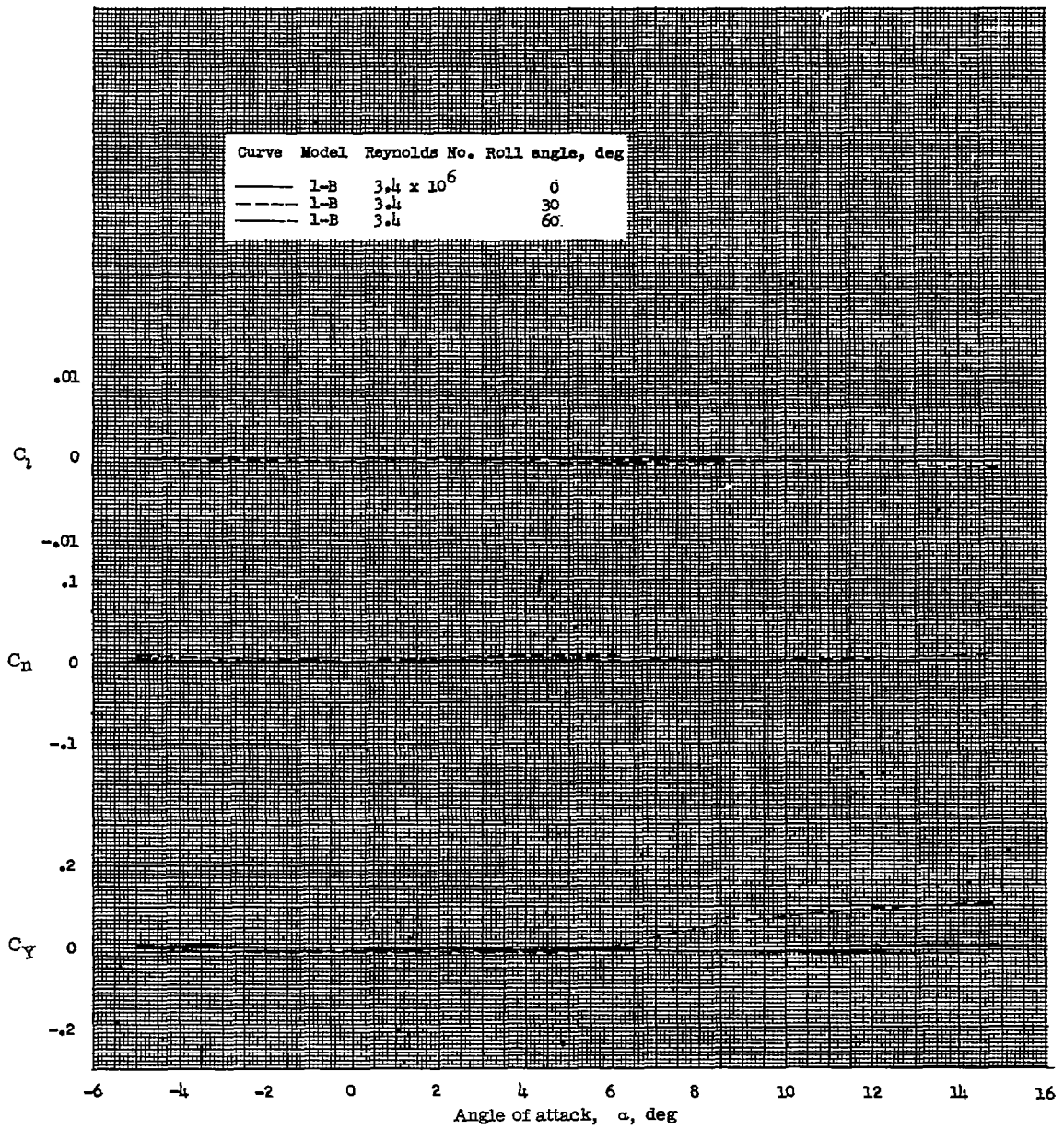

Figure 15.- Comparison of the lateral characteristics of configuration 1-B for various angles of roll. M = 6.86.

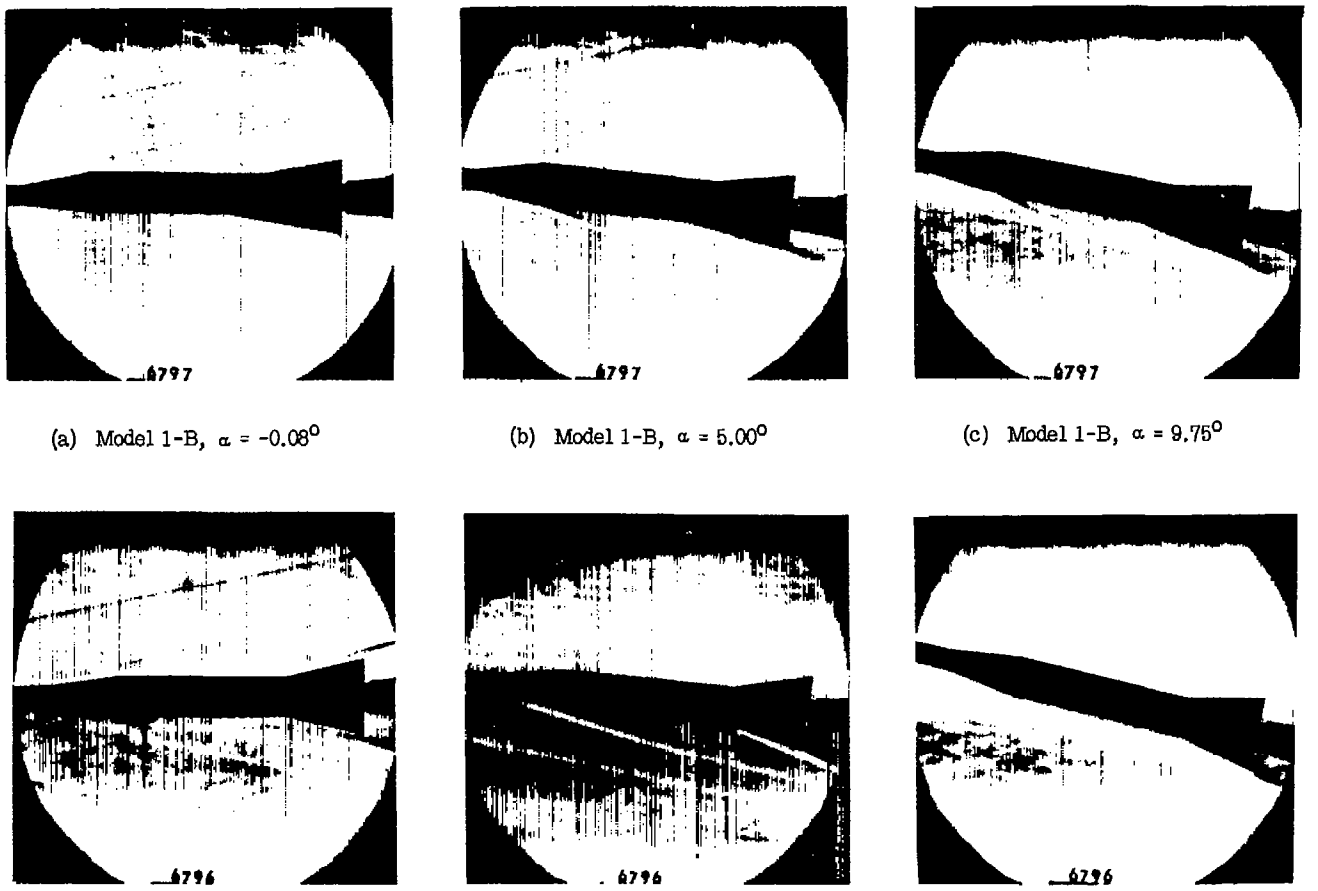

(a) Model 1-B, $\alpha = -0.08^{\circ}$ (b) Model 1-B, $\alpha = 5.00^{\circ}$ (c) Model 1-B, $\alpha = 9.75^{\circ}$

(d) Model 1-C, $\alpha = -0.42^{\circ}$ (e) Model 1-C, $\alpha = 5.08^{\circ}$ (f) Model 1-C, $\alpha = 12.40^{\circ}$

L-57-190

Figure 16.- Schlieren photographs of models 1-B and 1-C at various angles of attack. M = 6.86; roll angle, 0°; R, 3.4×10^{6}.

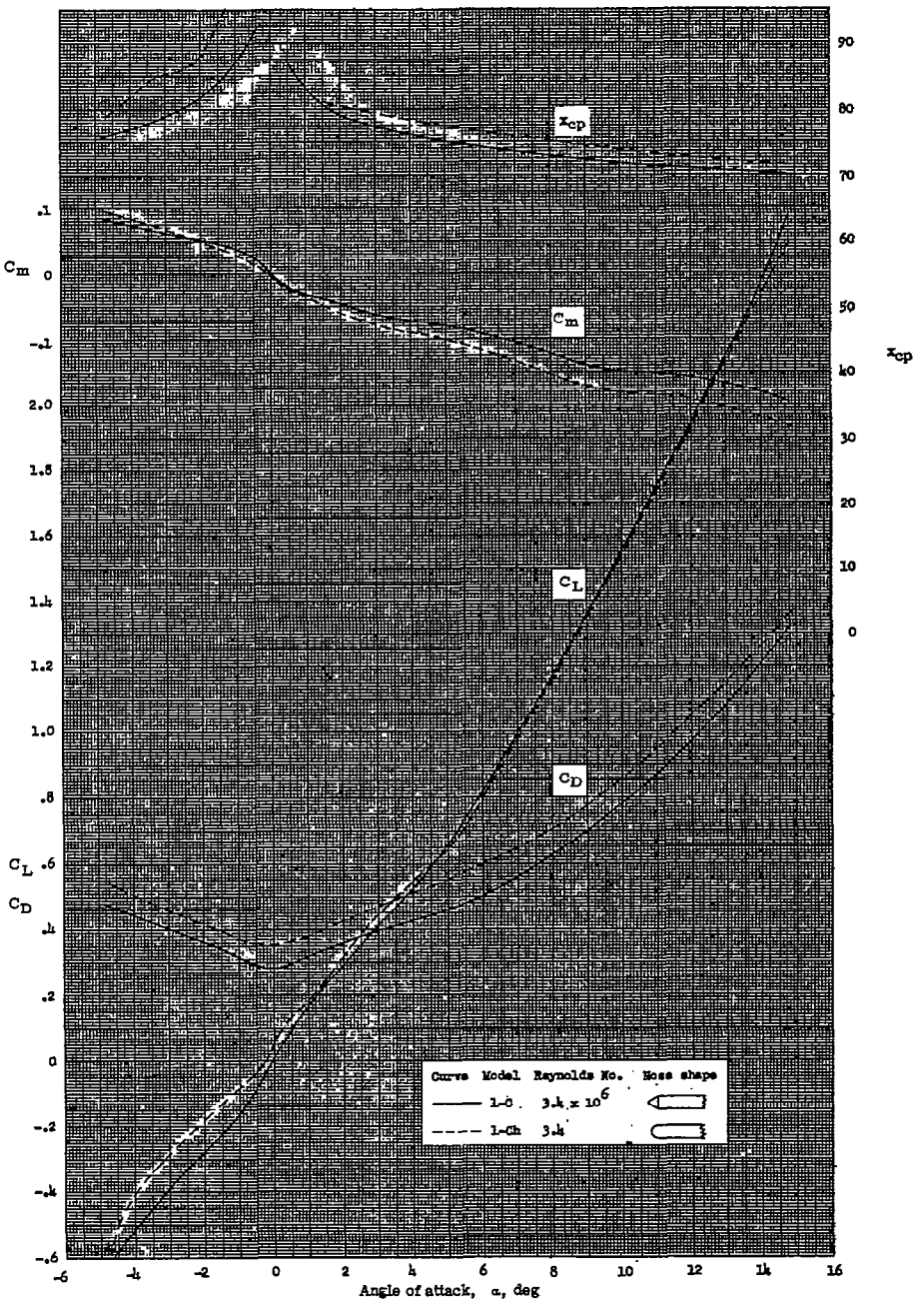

(a) Lift, drag, pitch, and center of pressure.

Figure 17.- Comparison of the longitudinal characteristics of configuration 1-C with and without hemispherical nose. M = 6.86.

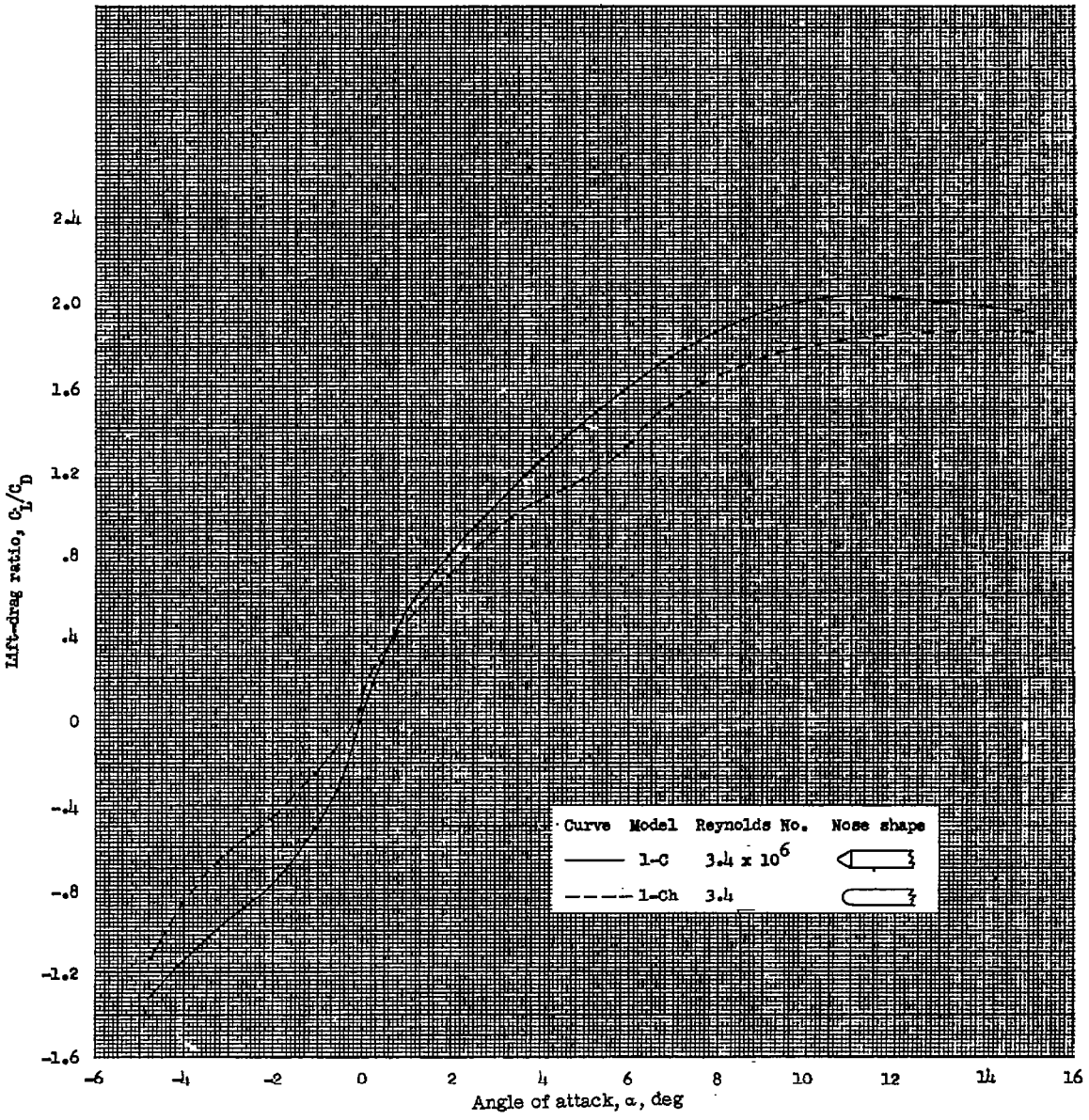

(b) Lift-drag ratio.

Figure 17.- Concluded.

[redacted]

[redacted]ld, Va.